Modeling Seasonal Effects of River Flow on Water Temperatures in an Agriculturally Dominated California River

J. Eli Asarian[1,1], Crystal Robinson[2,2], and Laurel Genzoli[3]

[1]Riverbend Sciences
[2]Quartz Valley Indian Reservation
[3]Flathead Lake Biological Station and the University of Montana

February 15, 2023

Abstract

Low streamflows can increase vulnerability to warming, impacting coldwater fish. Water managers need tools to quantify these impacts and predict future water temperatures. Contrary to most statistical models' assumptions, many seasonally changing factors (e.g., water sources and solar radiation) cause relationships between flow and water temperature to vary throughout the year. Using 21 years of air temperature and flow data, we modeled daily water temperatures in California's snowmelt-driven Scott River where agricultural diversions consume most summer surface flows. We used generalized additive models to test time-varying and nonlinear effects of flow on water temperatures. Models that represented seasonally varying flow effects with intermediate complexity outperformed simpler models assuming constant relationships between water temperature and flow. Cross-validation error of the selected model was [?]1.2 °C. Flow variation had stronger effects on water temperatures in April–July than in other months. We applied the model to predict effects of instream flow scenarios proposed by regulatory agencies. Relative to historic conditions, the higher instream flow scenario would reduce annual maximum temperature from 25.2 °C to 24.1 °C, reduce annual exceedances of 22 °C (a cumulative thermal stress metric) from 106 to 51 degree-days, and delay onset of water temperatures >22 °C during some drought years. Testing the same modeling approach at nine additional sites showed similar accuracy and flow effects. These methods can be applied to streams with long-term flow and water temperature records to fill data gaps, identify periods of flow influence, and predict temperatures under flow management scenarios.

Modeling Seasonal Effects of River Flow on Water Temperatures in an Agriculturally Dominated California River

J. Eli Asarian[1], Crystal Robinson[2†], Laurel Genzoli[3]

[1]Riverbend Sciences, Eureka, CA, USA, [2]Quartz Valley Indian Reservation, Fort Jones, CA, USA, [3]Flathead Lake Biological Station and the University of Montana, Missoula, MT, USA, [†]current affiliation: California Department of Fish and Wildlife, Yreka, CA, USA

Corresponding author: J. Eli Asarian (eli@riverbendsci.com)

Key Points:

- In this snowmelt and groundwater-influenced river, water temperatures stayed cool later into summer in high-flow years than low-flow years
- Statistical water temperature model predictions became more accurate when the influence of river flow was allowed to vary seasonally
- These accessible models can be applied to other rivers or streams with daily, long-term flow and water temperature records

Abstract

Low streamflows can increase vulnerability to warming, impacting coldwater fish. Water managers need tools to quantify these impacts and predict future water temperatures. Contrary to most statistical models' assumptions, many seasonally changing factors (e.g., water sources and solar radiation) cause relationships between flow and water temperature to vary throughout the year. Using 21 years of air temperature and flow data, we modeled daily water temperatures in California's snowmelt-driven Scott River where agricultural diversions consume most summer surface flows. We used generalized additive models to test time-varying and nonlinear effects of flow on water temperatures. Models that represented seasonally varying flow effects with intermediate complexity outperformed simpler models assuming constant relationships between water temperature and flow. Cross-validation error of the selected model was ≤1.2 °C. Flow variation had stronger effects on water temperatures in April–July than in other months. We applied the model to predict effects of instream flow scenarios proposed by regulatory agencies. Relative to historic conditions, the higher instream flow scenario would reduce annual maximum temperature from 25.2 °C to 24.1 °C, reduce annual exceedances of 22 °C (a cumulative thermal stress metric) from 106 to 51 degree-days, and delay onset of water temperatures >22 °C during some drought years. Testing the same modeling approach at nine additional sites showed similar accuracy and flow effects. These methods can be applied to streams with long-term flow and water temperature records to fill data gaps, identify periods of flow influence, and predict temperatures under flow management scenarios.

Plain Language Summary

Warm water temperatures threaten culturally and economically important salmon in Pacific Northwest rivers, causing chronic stress and direct mortality. Climate change and agricultural water use have reduced summer river flows in recent decades, intensifying water scarcity. Years with deep mountain snowpack and resulting high groundwater levels extend the high flow season and keep water temperatures cool through the end of July, whereas in drought years the river warms sooner. We used 21 years of river flow and air temperature data from the Scott River, California, to create computer models that simulate water temperatures. Our models allow the effect of flow on water temperatures to vary by season (i.e., stronger cooling effects in spring and summer), improving accuracy of the simulated temperatures. We used the Scott River model to simulate water temperatures under two alternative flow scenarios considered in local water management plans. Our simulations indicate that relative to current conditions, the higher flow scenario would lower the summers' highest temperatures and decrease the number of days that river temperatures exceed a biological threshold. Testing the same modeling approach at nine additional Klamath Basin sites showed similar accuracy and flow effects. Our model is freely available for public use.

1 Introduction

Water temperature in rivers and streams drive physical, chemical, and biological processes (Ouellet et al., 2020). Stream temperatures determine species ranges, with alterations to natural temperature regimes causing deleterious effects to native species (Wenger et al., 2011). Stream temperatures are widely altered by human activities (Webb et al., 2008). Maintaining ecological integrity is a major stream temperature management goal, yet models used to predict stream temperature response to management interventions either lack predictive power or are time-consuming to develop.

River flow rates (i.e., discharge) are a key driver of stream temperatures through multiple mechanisms. While stream temperatures are determined by surface and streambed energy fluxes and advected heat (Caissie, 2006; Moore et al., 2005), flows influence these factors and their effect on temperature. Higher flows generally increase water volume and thus a stream's capacity to store heat, reducing daily temperature fluctuations (Brown, 1969; Folegot et al., 2018; Meier et al., 2003; Sinokrot & Gulliver, 2000). Higher flows speed downstream transit of water, reducing the time that a parcel of water is exposed to ambient heating (or cooling) at a given location and increasing the influence of upstream conditions (Bartholow, 1991; Dymond J., 1984; Folegot et al., 2018). Channel geometry, including width/depth ratio, influences these effects (Dugdale et al., 2017).

The relationship between water temperature and flow varies through time. Seasonal changes in precipitation phase (i.e., snow and rain) affect water temperatures (Yan et al., 2021). The geographical source of water can shift seasonally, and can include tributaries, point sources, hillslopes, and alluvial aquifers, with each source having different temperatures and heating or cooling trajectories while en route to stream channels (Dugdale et al., 2017; Steel et al., 2017). Groundwater-surface water interactions and hyporheic exchange also affect temperatures (Hannah et al., 2009; Kurylyk et al., 2015). Water management, including reservoir releases, water withdrawals, and irrigation runoff can further alter temperature dynamics (Alger et al., 2021; Chandesris et al., 2019). Flow effects on water temperature are further mediated by seasonal changes to solar radiation received by the stream. Day length and solar angle, which affect topographic and riparian shading, remain consistent among years (Piotrowski & Napiorkowski, 2019; Yard et al., 2005). Other mediators of solar radiation including leaf out and leaf fall of deciduous riparian vegetation, cloud cover (Dugdale et al., 2017), water vapor, dust (Theurer et al., 1984), wildfire smoke (Asarian et al., 2020; David et al., 2018) and other aerosols follow seasonal trajectories that vary among years. Despite time-varying changes in how flow dynamics influence stream temperature, many stream temperature models do not account for these seasonal variations in the relationship between flow and stream temperatures.

Given stream temperature's importance and vulnerability to human alterations, water managers need tools to predict stream temperature changes associated with climate change and flow management (Gibeau & Palen, 2020; Null et al., 2017). While process-based (i.e., deterministic) models simulating stream energy budgets can have high predictive accuracy, their use is limited by extensive data input requirements (Brown, 1969; Caissie, 2006; Dugdale et al., 2017). Statistical models that use empirical relationships between stream temperature and environmental drivers require fewer input variables so are easier to implement, but for scenario prediction they are generally not considered as reliable as process-based models (Arismendi et al., 2014; Benyahya et al., 2007a; Caissie, 2006). However, statistical modeling methods have evolved, improving prediction accuracy and temporal resolution (i.e., daily) (Ouellet et al., 2020; Piotrowski & Napiorkowski, 2019). Year-round daily temperature models are especially valuable because they match the time scales used in detailed biological studies and water quality regulations (Imholt et al., 2010; Railsback et al., 2015; USEPA, 2003).

Statistical stream temperature models have long relied on air temperature as the primary predictor (Mohseni et al., 1998), but year-round daily models should incorporate additional mechanisms to improve accuracy and reflect physical processes (Letcher et al., 2016). Statistical stream temperature models use air temperature to represent net radiative flux (Caissie 2006). Time lags between air temperatures and water temperature reflect heat exchange processes (Koch & Grünewald, 2010; Soto, 2016; Webb et al., 2003), while temporal autocorrelation acknowledges that stream temperature on a given day is in part a result of stream temperature the previous day (Benyahya et al., 2007a, 2007b, 2008; Yang & Moyer, 2020). Inclusion of flow can improve model accuracy (Santiago et al., 2017; Sohrabi et al., 2017; van Vliet et al., 2011; Webb et al., 2003). The relationship between air and stream temperatures is nonlinear and differs among seasons (Arismendi et al., 2014, Caissie et al., 2001; Mohseni et al., 1998). Including time-varying effects could improve the predictive accuracy of stream temperature models across variable conditions.

Several methods allow seasonal variation in the relationship between environmental covariates and stream temperatures. These methods not only improve model accuracy but also identify the times when effects are strongest. While time-varying covariate effects can be represented using separate models for each season (Mohseni et al., 1998; Sohrabi et al., 2017), this may cause unnatural, abrupt changes at seasonal transitions. Time-varying coefficients, including those used in generalized additive models (GAMs) (Pedersen et al., 2019; Wood, 2017) use continuous functions that avoid these abrupt changes (Li et al., 2014; Jackson et al., 2018; Siegel & Volk, 2019). While GAMs have been used in daily stream temperature modeling for single-site prediction (Boudreault et al., 2019; Coleman et al., 2021; Glover et al., 2020; Laanaya et al., 2017; Siegel et al., 2022), spatiotemporal prediction (Jackson et al., 2018; Siegel & Volk, 2019), identifying extreme events (Georges et al., 2021), and trend assessment (Yang & Moyer, 2020), few studies have used GAMs to model seasonally varying flow effects or identify when stream temperatures are most affected by flow variation (Glover et al., 2020; Yang & Moyer, 2020). With flexible model structures and easy implementation, GAMs could be a powerful tool for predicting stream temperatures under flow management scenarios, but to our knowledge these models have not been previously used for this purpose.

Our objectives were to predict mean and maximum daily stream temperatures under management flow scenarios and new environmental conditions, and to identify periods when flow has the strongest influence on stream temperatures. We compared 11 GAM structures using flow, air temperature, and day of year as covariates that incorporated combinations of linear, nonlinear, and seasonally-varying effects. Our model selection and validation procedures included extrapolation tests evaluating predicted stream temperatures with flows and air temperatures outside the calibration range, designed to favor models that had enough complexity to represent the key patterns in the data, but not so complex that they overfit the data. We applied the top model to proposed management flow scenarios and extreme flow and air temperature conditions. The models are intended to be used as a tool to inform water management, making the relatively simple model structure and coding of GAMs our choice of modeling technique. We focused our analyses on the Scott River of Northern California, where low flows and high temperatures are limiting factors for coldwater fish and water managers are considering implementing regulations to protect instream flows. To demonstrate wider applicability, we evaluated similar models in nine additional sites in the Klamath River Basin.

2 Study Area

Our study area is the lower Klamath River Basin, California, USA, focusing on one large tributary—the Scott River (Figure 1). The Scott River study site is located at the outlet of Scott Valley, with a drainage area of 1,714 km^2. The other nine sites are near USGS gaging stations with drainage areas ranging from 58 km^2 to 31,300 km^2 (Figure 1, Table S1). The climate is Mediterranean with precipitation occurring primarily in winter and spring as rain at low elevations and snow at higher elevations (VanderKooi et al., 2011). The human population lives primarily on private land along watercourses including Scott Valley, where irrigated agriculture dominates land use, utilizing groundwater and surface water (Foglia et al., 2018). The Scott River has no major dams or reservoirs, but there are large dams on the Klamath River and two tributaries (Shasta and Trinity rivers), influencing some study sites.

The Scott Valley aquifer fills during the high flows of winter rainstorms and spring snowmelt-driven runoff. As runoff recedes through summer, most surface water is diverted for irrigation and river water at the Scott Valley outlet becomes increasingly composed of groundwater from valley alluvium. Minimum flows occur in early September before rising due to fall rains (Figure 2b). In late summer of drought years, portions of the Scott River have no surface flow (Tolley et al., 2019). Summer and fall river flows have declined in recent decades (Kim and Jain, 2010; Asarian and Walker, 2016) due to a combination of climate change (Drake et al., 2000) and increased groundwater withdrawals, especially since 1977 (Van Kirk and Naman, 2008). Climate change is expected to further reduce flows by decreasing snowpack and increasing irrigation demand (Persad et al., 2020).

Management flows have been proposed for the Scott River to protect Endangered Species Act-listed coho salmon (*Oncorhynchus kisutch*) and other coldwater salmonid fishes. These fishes' importance to local Native American tribes has led to contention over water management. River water temperatures in May–July are much cooler in high-flow years than low-flow years (Figure 2), and water extraction has contributed to the Scott River being listed as impaired for water temperature under the Clean Water Act (NCRWQCB, 2005). The U.S. Forest Service has a first-priority Schedule D water right for Scott River instream flow that varies by month and day from 30–200 ft^3/s (0.85–5.67 m^3/s) (Superior Court of Siskiyou County, 1980) (Figure 3b), but does not exercise its legal authority to curtail lower-priority water uses when flows drop below these levels. The California Department of Fish and Wildlife (CDFW) proposed interim Scott River instream flow targets that vary by month and day from 62–362 ft^3/s (10.3–1.75 m^3/s) (CDFW, 2017) (Figure 3b), but these have no legal force.

3 Methods

At each of the 10 sites, we developed GAMs to predict daily mean stream temperature (T_{mean}) and daily maximum stream temperature (T_{max}) using flow, air temperature, and day of year as covariates. We compared models across a range of complexity, including those with seasonally varying flow effects, to models with a constant relationship between stream temperature and flow. We selected a final model based on the best overall performance averaged across the 10 sites. We then applied that model to flow management scenarios at one site– the Scott River.

3.1 Data sources and preparation

3.1.1 Water temperature and river flow

We obtained water temperature data from six sources (Table S1). For the Scott River site, we used Quartz Valley Indian Reservation (QVIR) (QVIR, 2016; Asarian et al., 2020) data, supplemented by U.S. Forest Service (USFS) (KNF, 2010, 2011) and U.S. Bureau of Reclamation (USBR) (Smith et al., 2018) data. For the nine other sites, we used data from the U.S. Fish and Wildlife Service (USFWS) (Manhard et al., 2018; Romberger & Gwozdz, 2018), USFS (KNF, 2010, 2011), USBR, U.S. Geological Survey (USGS), and California Department of Water Resources (CDWR). Equipment calibration information is provided in Text S1. Following compilation, we reviewed the data and removed any suspicious values (e.g., when there were calibration issues or probes appear to have been exposed to air). We then calculated T_{mean} and T_{max}. For days when data were available from multiple entities, we averaged values (Text S1). Data availability at each site ranged from 3,540–5,684 days and 16–21 years (1998–2020), with at least five days of data for every julian day. We paired daily temperatures at each site with daily average streamflow data from nearby USGS gages (Figure 1, Table S1).

3.1.2 Air temperature

We retrieved daily mean air temperatures for each site from the 4-km resolution gridded PRISM dataset (Daly et al., 2008). Because stream temperatures are correlated with air temperature at multiple time scales, we initially explored many metrics (Piotrowski & Napiorkowski, 2019). In these initial explorations at Scott River, we found that two-day weighted air temperature (A_{2w}) resulted in good model fits (Text S2), so we used A_{2w} for all models except one that used a seven-day average (A_7) to mimic Mohseni et al.'s (1998) widely-implemented model. A_{2w} is calculated as follows, where A is mean air temperature on day *i*:

$$A_{2w} = \frac{A_i + (0.5 \times A_{i-1})}{1.5} \tag{1}$$

To improve numerical stability, we standardized air temperature (°C) and flow (log10 m^3/s) by centering and scaling (i.e., subtracting the mean, then dividing by the standard deviation).

3.1.3 Flow and air temperature quantiles

At each site, we used smooth additive quantile regression models (Cade and Noon, 2003; Fasiolo et al., 2020) to calculate the air temperature associated with three quantiles (0.1, 0.5, and 0.9, equivalent to 90%, 50%, 10% exceedance probabilities) for each day of the year (Figure 3a), using the qgam R package (Fasiolo et al., 2020) with a 12-knot cyclic cubic regression spline ("cc"). We refer to the 0.1, 0.5, and 0.9 air temperature quantiles as Coolest, Typical, and Hottest, respectively. We also derived three flow quantiles, with the 0.1 quantile representing Lowest flows, 0.5 quantile representing Typical flows, and the 0.9 quantile representing Highest flows (Figure 3b). These quantiles were used to generate model scenarios (Section 3.4).

We used similar quantile regression models at each site to categorize each date into one of nine categories based on combinations of flow quantiles (High is >0.67 quantile, Moderate is 0.33–0.67 quantile, Low is <0.33 quantile) and air temperature quantiles (Cool is <0.33 quantile, Moderate is 0.33–0.67 quantile, Warm is > 0.67 quantile). These categories were used to define cross-validation blocks (Section 3.3).

3.2 Model development and calibration

At each of the 10 sites, we developed 11 models of T_{max} and T_{mean} using combinations of river flow, air temperature, and day of year (D) as covariates, including interactions (Figure 4). Models are numbered according to effective degrees of freedom for fixed effects, from most complex (GAM1) to least complex (GAM11). GAMs were developed in the mgcv R package version 1.8-41 using the bam function (Wood, 2017), fit using fast restricted maximum likelihood (fREML). Model terms were either linear coefficients or smooth non-linear functions with wiggliness determined by a smoothing penalty (Pedersen et al., 2019; Wood, 2017). We used cyclic cubic regression splines ("cc") as the smoother for D and thin plate regression splines ("tp") as smoothers for other covariates. To improve prediction under new conditions and avoid overfitting (Jackson et al., 2018; Siegel & Volk, 2019), we limited smoothers for air temperature and flow to a maximum of three knots, except in the one-covariate model "GAM11" where air temperature was allowed six knots. D was allowed up to six knots, except in three-dimensional tensors where it was restricted to five knots.

Some models included interactions between D and other covariates (i.e., flow or air temperature) to allow that covariate's effect to vary seasonally. These interactions were either partially nonlinear or fully nonlinear. For partially nonlinear interactions, the linear slope of one variable (e.g., flow) varied as a smooth nonlinear function of D (Jackson et al., 2018, Siegel & Volk, 2019). Fully nonlinear relationships between two or more variables were specified as tensor product smooths or tensor product interactions (Wood, 2017).

All models except "GAM11", the simplest model structure tested, included an AR-1 autocorrelation error structure and a random effect for year. We initially fit each model without an autocorrelation term, then re-fit with an autocorrelation term, assigning a rho value based on the initial model's lag-1 autocorrelation (Baayen et al., 2018; van Rij et al., 2019, 2020) (Text S3).

Since Mohseni et al.'s (1998) nonlinear logistic regression of weekly air temperature and stream temperature has been widely applied and adapted (Piotrowski & Napiorkowski, 2019), we included a GAM equivalent of it as a benchmark for comparison. A_7 is the only predictor in this "GAM11" model (i.e., no flow, autocorrelation, or random effects).

We reviewed residual plots and autocorrelation function plots to verify assumptions. We evaluated each model's concurvity using mgcv's concurvity function.

3.3 Model selection and validation

We used cross-validation (CV) for model selection and validation because it is preferred over information theoretic approaches when prediction is paramount (Pedersen et al., 2019). We designed extrapolation CV tests to select models that performed well when applied to environmental conditions (i.e., flow and air temperature) outside the calibration range (Lute & Luce, 2017; Roberts et al., 2017). We split data into blocks based on quantiles of flow and air temperature (Section 3.1.3), withheld one block, and fit the model using the remaining block (Figure 5). We compared predictions for the withheld blocks against the measured data using root mean squared error (RMSE). These dual-variable differential split-sample tests (Klemeš, 1986) extrapolate not only into new combinations of flow and air temperature but also into new ranges of both individual variables.

We selected the best model by ranking the 11 candidate models (GAM1–GAM11) based on their extrapolation test RMSE values for each site and each temperature response variable (10 sites, 2 variables). We then calculated the mean of the 20 ranks for each candidate model, selecting the model with the lowest mean rank. We selected the same model structure for T_{max} and T_{mean} (rather than optimizing separately) so predictions for both metrics could be used together. We present Bayesian information criterion (BIC) scores from models fit using maximum likelihood, to compare our extrapolation-based model selection to more commonly applied—and easier to implement—model selection methods. To facilitate comparisons to previous studies, we also use leave-one-year-out (LOYO) CV where data were split into annual blocks and then treated similarly to the extrapolation tests (i.e., steps repeated for each year: year withheld, model refit using remaining data, and predictions compared to withheld data). We assessed the relative importance of individual model terms by comparing performance among models with and without individual predictors and/or interactions.

3.4 Model scenarios assessing management effects and timing of flow importance

3.4.1 All sites

To assess the seasonal response of stream temperatures to variation in flow and air temperatures, we applied our selected model to scenarios representing differing air temperatures and flows (Table 1, Figure 3). We ran nine "quantile air temperature" scenarios representing combinations of three air temperature inputs (0.1, 0.5, and 0.9 quantiles) and three flow inputs (0.1, 0.5, and 0.9 quantiles) (Section 3.1.3) for each site. Replication is sparse for the co-occurrence of extreme quantiles of both air temperature and flow (e.g., mean 4.9 days of record per month and site with flow ≤0.1 quantile and air temperature ≥0.9 quantile); however, ample data are available in nearby quantiles (e.g., mean 19.1 days per month and site with flow ≤0.2 quantile and air temperature ≥0.8 quantile) (Figure S1).

3.4.2 Scott River

At Scott River only, six additional scenarios were run that paired the three quantile air temperatures with the USFS water right and CDFW flow criteria (Section 2) as flow inputs (Table 1, Figure 3). The CDFW and USFS flows are aligned with extreme drought conditions in April and May (0.1 quantile) and high flows in August and September (0.5 to 0.9 quantile).

We also applied our selected model to "observed air temperature" scenarios that pair observed air temperatures for dates 1998–2020 with eight flow conditions for the Scott River: observed USGS flows, the five flows from the "quantile air temperature" scenarios (Lowest, Typical, Highest, USFS, and CDFW), and two additional scenarios in which the CDFW and USFS flows were replaced by observed USGS flows on dates when the observed flows were higher than the management flows (Table 1). Using observed air temperatures instead of quantile air temperatures provides more realistic predictions because air temperatures fluctuate from day to day (Figure 2a), instead of remaining near the same quantile like flow does during May–September recession. We summarized the results of each "observed air temperature" scenario by calculating: 1) annual maximum temperature, 2) first and last day each year in which water temperatures exceed 22 °C, and 3) the annual degree days exceedance of 22 °C, calculated by subtracting 22 from all T_{max} and summing all positive values. We chose 22 °C as an indicator of biological effects on juvenile salmonids, based on geographically proximal studies (Brewitt and Danner, 2014; Sutton et al., 2007; Sutton & Soto, 2012) (Text S4).

4 Results

4.1 Model selection and validation

GAM7 had the lowest mean rank RMSE in extrapolation CV (Table S2), so was selected as our final model. GAM7 had an all-site RMSE of 1.15 °C for T_{max} and 1.01 °C for T_{mean}, and had the lowest RMSE at Scott River (T_{max} 1.20 °C, T_{mean} 1.00 °C) (Figure 4). GAM7 features nonlinear smoothers for day of year (D), two-day weighted air temperature (A_{2w}), and flow (Q); a nonlinear smoother of D interacted with linear Q (i.e., linear slope of Q varies by D); and a nonlinear smoother of D interacted with linear A_{2w} (Figure S3, Figure 6). GAM7 had intermediate complexity, with 12.6 effective degrees of freedom for fixed effects for Scott River T_{max}, compared to 23.6 for the most complex model (GAM1), and 5.8 for the least complex model (GAM11) (Figure S4).

Extrapolation CV showed that at all sites, including Scott River, models with seasonally varying flow effects had much higher accuracy than models lacking that feature (Figure 4). For example, for T_{max}, all-site RMSE was 1.15–1.19 °C for models with seasonally-varying flow effects (GAM1–GAM8) and 1.67 °C for GAM9 that lacked seasonally varying flow. Models lacking flow (i.e., containing only D or A_{2w}) performed the worst, with all-site RMSE values of 1.74 °C and 2.25 °C for GAM10 and GAM11, respectively, for T_{max}. GAM7's combination of a nonlinear smoother for flow and a partially nonlinear interaction of flow and D represented flow effects well, given that the additional complexity of tensors (fully nonlinear interactions of flow and D) in GAM1–GAM5 did not substantially improve model performance at most sites. Models interacting flow and air temperature (i.e., GAM1 and GAM4) did not outperform GAM7 which lacked this interaction. BIC scores largely corroborate the extrapolation CV results identifying the importance of seasonally varying flow effects and top ranking of our extrapolation CV-selected model GAM7 (Text S5, Figure S4).

Scott River GAM7 LOYO CV predicted overall seasonal patterns in measured T_{max} for dates stratified into combinations of differing quantiles of air temperatures and flows. RMSE was higher for dates with low (<0.33 quantile) flows (Figure S2c). T_{max} Scott River GAM7 extrapolation CV prediction accuracy was only slightly lower than LOYO CV prediction accuracy when averaged over the entire year (i.e., RMSE 1.20 °C vs. 1.18 °C, Figure 4), but were biased low during May and June during high (>0.67 quantile) flows, having only been calibrated with data from the low-flow and moderate-flow quantile (Figure S5). Complete time series of Scott River measured and LOYO CV T_{max} and T_{mean} for all years are shown in Figures S6–S7.

4.2 Model scenarios assessing management effects and timing of flow importance

Water temperature predictions under quantile air temperature scenarios on the Scott River using our selected model (GAM7) showed water temperatures responded to changes in flow across all quantiles of air temperature, consistent with measured data (Figure S2). Cooling effects of flow followed a seasonal pattern, rising in March to reach maximum effect size on 15 June (7.7 °C for T_{max} and 5.5 °C for T_{mean}), then diminishing to near zero by early September (Figure 7). Consistent with measured data (Figure S2), modeled annual maximum water temperatures occurred later in the season in high-flow conditions (i.e., late July or early August) than in low-flow conditions (i.e., early/mid-July) (Figure 7).

Timing and magnitude of flow effects varied among the 10 Klamath Basin sites, but generally followed a similar seasonal trend of flow having the strongest cooling effects in April–July, less cooling effects in March and August, and warming effects in November through February (Figure 8). Cooling effects of flow were strongest at Scott River and weakest at Shasta River.

The Scott River "observed air temperature" scenarios, which paired observed air temperatures with eight flow scenarios, demonstrated how flow variation influences stream temperature timing and magnitude. The lowest flow scenario (0.1 quantile) had annual maximum temperatures 3.3 °C warmer than the highest flow scenario (0.9 quantile) (Figure 9a), and first reached 22 °C 48 days earlier (Figure 9c). The last day with temperatures >22 °C differed by only 2 days (Figure 9d). The observed scenario had the most interannual variation in annual maximum temperature (Figure 9a) and timing of exceedances of 22 °C (Figure 9c,d), because it included very low flows and very high flows. Predicted temperature responses to the CDFW and USFS flow scenarios are complex and depend on how the flows are implemented. If implemented as bypass flows, above which all additional water is diverted, then temperatures reached 22 °C *earlier* than the observed flow scenario by 4 days for the CDFW flows and 13 days for USFS flows (Figure 9c and Figure S8) because these management flows are lower than observed flows in May and June (Figure 3). However, in the scenarios where the CDFW and USFS flows were replaced by observed USGS flows on dates when the observed flows were higher than the management flows, then predicted temperatures reached 22 °C *later* than the observed scenario by 4 days with CDFW flows and 2 days with USFS flows. In addition, the number of years with exceedances of 22 °C prior to 23 June were reduced from 7 to 0 (Figure 9c) because CDFW flows were higher than observed flows in drought years. Due to higher July and August flows, annual maximum water temperatures were 1.0–1.1 °C cooler in the CDFW scenarios than the observed flow scenario (Figure 9a). Differences in annual degree-days exceedance of 22 °C between scenarios (Figure 9b) were similar to annual maximum temperature.

5 Discussion

At all 10 sites, models with seasonally varying flow effects substantially outperformed models with a constant relationship between stream temperature and flow, indicating that the influence of flow changes throughout the year. Models containing only air temperature performed particularly poorly because they did not include flow as a covariate, while models with a linear effect of flow had intermediate accuracy. Flow had the strongest effect on water temperatures in

April–July. The highest Scott River management flow evaluated would substantially decrease exceedances of 22 °C and reduce annual water temperature maximums.

5.1 Model selection and performance

Model accuracy of our top model and similar model structures were high for both T_{max} and T_{mean}. For T_{mean}, our selected model's LOYO CV RMSE ranged from 0.80–1.17 °C at 10 sites (Figure 4), better than the 0.75–1.75 °C RMSE in Mohseni-based models at 14 sites within our study area (Manhard et al., 2018). In additional to outperforming other models applied within our study area, our selected T_{mean} model also had better LOYO CV RMSE than most single-station year-round daily statistical models from around the world (all-site average model validation RMSE for each analysis's best performing class of models: Ahmadi-Nedushan et al. [2007] 0.51 °C, Boudreault et al. [2019] 1.45 °C, Coleman et al. [2021] 1.3 °C, Koch and Grünewald [2010] 1.25 °C, Laanaya et al. [2017] 1.44 °C, Letcher et al. [2016] 1.16 °C, Siegel et al. [2022] 0.87 °C, Sohrabi et al. [2017] 1.25 °C, van Vliet et al. [2011] 1.8 °C, and Soto et al. [2016] 1.20 °C). Our high model accuracy was achieved despite using PRISM air temperatures instead of local measurements—favoring ease of replicability.

GAMs were a useful modeling approach because they represented the nonlinear relationships and interactions between stream temperature and covariates. Our approach used >15-year calibration datasets spanning environmental conditions (i.e., hot and cool air temperatures and high and low flows). We prevented overfitting by restricting the number of knots in GAM smoothers (Section 3.2), basing model selection on extrapolation tests that evaluate prediction under expanded ranges of covariates (Section 3.3), and confirming that covariate responses and interactions matched scientific hypotheses regarding underlying physical processes (Section 5.3). Our selected model, GAM7, represented flow with two terms—a nonlinear smoother and a partially nonlinear interaction between flow and day of year—whose combined effects (Figure 6) provided enough flexibility for accurate predictions without overfitting. This two-term structure incrementally improves upon previous methods for representing flow effects, with GAM7's all-site extrapolation CV RMSE 0.04 °C better than GAM6, the model with a simpler flow effects structure nearly identical to Glover et al. (2020). Consistent with warnings from Siegel & Volk (2019), tensors (fully nonlinear interactions) were too flexible and did not perform as well as GAM7 when applied to conditions differing from the calibration dataset (i.e., extrapolation tests), although tensor models still outperformed models without seasonally varying flow effects.

We used extrapolation CV for model selection, which required far more effort than BIC-based selection. Since BIC scores suggested selection of the same model, GAM7 (Text S5), from an ease-of-use perspective BIC-based model selection appears preferable for future applications. However, for applications requiring high confidence in model accuracy, the extrapolation tests effectively demonstrate the ability to predict under new conditions.

5.2 Magnitude and timing of flow effects on water temperature

Consistent with physical expectations, our results corroborate previous findings from northern temperate rivers that during seasons when air temperatures are typically high and flows are typically low (i.e., summer in our study area), lower flows are often temporally correlated with higher stream temperatures (Arora et al., 2016; Isaak et al., 2017; Luce et al., 2014; Neumann et al., 2003), and flow more strongly affects T_{max} than T_{mean} (Asarian et al., 2020; Gu and Li, 2002;

Gu et al., 1998). In our study streams, high flows had a strong cooling effect on stream temperatures in April–July, but less influence during other months. Multiple linear regression (MLR) models using monthly flow and air temperature at 239 Northwestern USA sites not regulated by dams (Isaak et al., 2018) and spatial stream network models for eight regions of the Western USA (FitzGerald et al., 2021) showed monthly timing and direction of flow effects on stream temperatures (Figures S9–S10) similar to our results (Figure 8b), with the exception of similar cooling in April and August whereas our models show weaker cooling in August than in April. Monthly MLR modeling in 17 sites in Canada's Frasier River Basin found flow-mediated cooling effects on summer water temperatures were stronger in July than August and weakest in September (Islam et al., 2019). In Poland, where inter-season flow differences are less pronounced than in our study area, high flows were correlated with cooler water temperatures in April–September, with the strongest relationships occurring in July–September at mountainous snowmelt-fed rivers (Wrzesiński and Graf, 2022). An Eastern USA river study using a daily year-round GAM found that water temperature decreased with increased flow from April through mid-October (Yang & Moyer, 2020). Previous studies evaluating year-round changes in the relationship between stream temperature and flow generally used monthly time steps. Our daily model provides a more nuanced understanding of seasonal dynamics by allowing this relationship to change smoothly at sub-monthly time scales, facilitating identification of changes within a month, as well as the rate of change.

Flow-induced cooling in snowmelt-dominated rivers is common. Process-based modeling of a Sierra Nevada river indicated early summer stream temperatures up to 16 °C cooler in a record wet year relative to a dry year (Null et al., 2013). In steep Alaskan streams, average summer stream temperatures were 3–5 °C cooler in high-snowpack years than low-snowpack years (Cline et al., 2021). In the conterminous USA, including flow as a covariate improved daily stream temperature predictions over air temperature only models in April–August, but only in snowmelt-dominated streams (Sohrabi et al., 2017). Stronger flow effects occurred in inland regions than coastal regions of the Western USA (Figure S10) (FitzGerald et al., 2021), consistent with a greater percent of precipitation falling as snow (Klos et al., 2014). Climate change studies have not parsed the separate influences of hydrology and air temperature on stream temperature, but in snowmelt-dominated areas of western North America, predictions for disproportionate spring and summer stream temperature warming are nearly ubiquitous and attributed to snowpack declines causing lower flows in those seasons (Caldwell et al., 2013; Crozier et al., 2020; Ficklin et al., 2014; Leach & Moore, 2019; Lee et al., 2020; Luo et al., 2013; Null et al., 2013).

5.3 Model correspondence to physical mechanisms

We used air temperature and flow as the major predictors in our model, recognizing that these predictors represent many processes that collectively determine stream temperatures. Air temperature is not the most important component of stream heat budgets (Johnson, 2004; Dugdale et al., 2017), but it has high predictive power because it is correlated with net radiative flux, a key driver of stream heat budgets (Caissie 2006). Air temperature data resulted in high model accuracy in our study, and are widely attainable unlike radiative fluxes.

The effects of flow on stream temperature vary throughout the year in response to the physical mechanisms affecting stream energy balances. High flows speed downstream transit of water and provide increased thermal mass that resists heating (or cooling). While flow has strong effects on water temperature in April–July in our study area, its effects are substantially weaker—though still present—in August. High flow can exert a dominant influence on water temperature, but this influence wanes as flow recedes, leading to progressively greater influence of solar radiation and air temperature. The relationship between flow and water temperature in our top-preforming model is nonlinear and varies with day. Marginal effects of decreasing flow diminish as flow approaches 0 m^3/s (Figure 6). At Scott River, August flows were much lower than July (Figure 2, Figure 6), and by 15 August were always below 2.6 m^3/s (92 ft^3/s). These low August flows have shallow water depth, low thermal mass, and slow transit times resulting in residence time sufficient for water to heat up to equilibrium temperature (Bogan et al., 2003; Nichols et al., 2014; Tague et al., 2007). During hot, dry conditions such occurs in our study area during summer, evaporative cooling limits how high stream temperatures can rise even when flows are extremely low (Mohseni & Stefan, 1999; Mohseni et al., 1998; Shaw et al., 2017). Wildfire smoke could also reduce warming of August stream temperatures (David et al., 2018). Widespread fire is more likely during drought conditions (Westerling, 2016), suggesting potential for smoke to confound low flow effects on temperature by decreasing solar radiation. We did not include smoke in our models because the data are difficult to process and we wanted easily replicable methods, but smoke effects on stream temperatures peaked in August in our study area (Asarian et al., 2020). With less solar radiation and cooler air temperatures than earlier months, T_{max} is almost always less than 22 °C at Scott River by early September regardless of flow (Figure 7). In October–November, a period of hydrologic transition when precipitation ends seasonal baseflow recession, flows had little influence over stream temperature (Figure 8), but Scott River and two other sites had weak, modal flow-temperature relationships (i.e., highest water temperatures at moderate flows) (Text S6).

Groundwater contributes to the relationship between flow and stream temperature at our Scott River site, as it does in many rivers (Briggs et al., 2018; Isaak et al., 2017; Kelleher et al., 2012; Mayer, 2012; Nichols et al., 2014). Thermal infrared imagery, field measurements (NCRWQCB, 2005), and a groundwater model (Tolley et al., 2019) confirm that the 10 km of river directly upstream of our study site are a gaining reach where valley constriction forces substantial groundwater into the Scott River, a common phenomenon at the outlet of alluvial valleys (Stanford and Ward, 1992). Scott River flows are driven by a mix of valley groundwater dynamics and snowmelt-driven mountain runoff (Foglia et al., 2013; Van Kirk and Naman, 2008). As mountain runoff recedes and tributaries are almost fully diverted for irrigation, the relative contribution of groundwater to surface flow at the valley outlet increases over the summer and becomes dominant (NCRWQCB, 2005). Sediments underlying the river and its tributaries have high hydraulic conductivity, so groundwater and surface water are strongly connected (Tolley et al., 2019). During the May–September recession period when temperatures are of greatest biological concern, flows are related to aquifer levels, and the relative proportions of valley outlet flow derived from mountain runoff and groundwater are well-predicted by flow and day of year. Thus, even though these two sources have different temperatures and our model does not explicitly differentiate them, the model performs well because the interaction of flow and day of year implicitly characterizes these dynamics adequately. Scenarios from a short-term process-based surface water model predicted doubling groundwater-derived flow would cool 30 July 2003 Scott River T_{max} by 2 °C, and a 50% reduction of groundwater-derived flow would warm temperatures by 2 °C (NCRWQCB, 2005). For comparison, applying our model to scenarios doubling or halving the 3.03 m^3/s (107 ft^3/s) gaged flow for that same date predicts T_{max} 1.0 °C cooler or 0.7 °C warmer, respectively.

Statistical models typically require many fewer variables as data inputs than process-based models do, so are often much simpler to develop (Caissie, 2006; Ouellet et al., 2020); however, this ease has tradeoffs. For example, our model does not differentiate between specific sources of inflows, which may have quite different temperature influences, nor how alternative management scenarios would spatially and temporally alter those inflows. If fundamental characteristics of valley hydrology (i.e., management or climate) changed dramatically, model accuracy could suffer. Similarly, applying the model to covariate combinations beyond those used in calibration will degrade predictive accuracy (Section 5.5). To avoid overly complex models that overfit calibration data, we used extrapolation tests to favor selection of simpler more generalizable models. Our model does not incorporate longer-term (e.g., annual to decadal) variation in air temperature that affects groundwater temperatures and precipitation phase (e.g., snow or rain), so may underestimate responses relative to predictions from integrated process-based models (Leach & Moore 2019).

5.4 Biological implications

Higher Scott River flows extend the period when cool water habitat is available (Figure 9), giving juvenile salmonids additional time to migrate downstream and reduce thermal stress for fish that rear in the Scott River through the entire summer. Climate change will likely continue to reduce snowpack and summer flows (Persad et al., 2020), increasing duration of detrimentally warm temperatures. Mean diel range in June–August exceeds 5 °C, providing hours daily with temperatures <22 °C even when T_{max} exceeds 22 °C. Salmonids can potentially persist by using thermal refugia where cool tributaries, groundwater, or hyporheic flow enters the river during hotter hours and then forage in the mainstem when temperatures are cooler (Brewitt and Danner, 2014; Sutton et al., 2007; Sutton & Soto, 2012). However, substantial portions of the Scott River and tributaries lack surface flow during summer, especially in dry years, reducing habitat connectivity.

5.5 Applications and management implications

These models can be used not only to identify the seasonally varying influence of flow, but also to predict future stream temperatures based on managed flow recommendations and to impute missing data. Instream flow management frameworks are evolving (Mierau et al., 2017; Poff et al., 2017; Yarnell et al., 2020) and accurate stream temperature models provide a valuable tool to predict management outcomes.

Our modeling approach could facilitate water managers' ability to include stream temperature as a management target in areas that do not currently have operational process-based models. For example, Siskiyou County is developing a groundwater sustainability plan for the Scott Valley (Foglia et al., 2018). The current groundwater model does not simulate water temperatures (Tolley et al., 2019). Our model can be used to predict effects of flow on Scott River temperatures, including the CDFW and USFS flow thresholds under consideration, and could inform state agencies' development of new flow objectives. The CDFW and USFS flows were both predicted to cool maximum annual temperatures relative to current conditions, but improvements would be greater with the higher CDFW flows (Figure 9). We caution that while the CDFW and USFS flows are higher than typical observed flows in late summer and early fall, for March to early June they represent extreme drought conditions that could cause earlier exceedances of 22 °C (Figure 2b). Surface water diversions for in lieu recharge (switching irrigation source from groundwater to surface water) or managed aquifer recharge (Dahlke et al., 2018; Foglia et al., 2013) should not use the CDFW and USFS flows to guide maximum diversion rates, but instead be tailored to reduce deleterious effects on instream habitat including temperatures, such as ceasing diversions by 1 June, the first date when measured (Figure 2) and modeled temperatures (Figure 9) reach 22 °C.

As with any statistical model, prediction accuracy will degrade when applied to conditions more extreme than those present in the calibration dataset. Our selected model interacts day of year with flow and air temperature, so extrapolation caution applies not just to the range of individual variables but also their combined distributions. Our calibration dataset includes a wide range of hydrologic conditions, but no years without surface water diversions or groundwater pumping because those activities occur every year. Streamflow depletion from groundwater pumping is greater in dry years than wet years (Foglia et al., 2013). Simulated total valley-wide streamflow depletion peaks around 150,000 m^3d^{-1} (60 ft^3/s) in July–August (Foglia et al., 2013), exceeding streamflow in dry years. Our model should be suitable for modeling dry years for scenarios with reduced pumping and/or diversions, which would presumably have flows similar to existing wet years (and hence are within the range of calibration flows); however, in wet years such scenarios would likely exceed the range of calibration flows and therefore be subject to more uncertainty. Future application to scenarios with flows higher than observed should be interpreted with appropriate caveats.

Flow records are typically less available than water temperature records, so may constrain where our modeling approach can be applied. However, if site-specific flows were not available, data from a nearby site could be used if they were likely to be highly correlated (i.e., similar watershed characteristics). We did not systematically explore that issue, but the one site (South Fork Trinity River) where we used flows from an upstream station had prediction accuracy similar to the other nine sites (Figure 4). In addition, although our modeling approach should work well with records shorter than the >15-year datasets we used, we recommend further research to determine the minimum required period of record.

These models can also be used to fill gaps in stream temperature data records needed for other analyses (Glover et al., 2020). Their high accuracy suggests they would compare well with imputation methods used in recent daily year-round stream temperature analyses (Isaak et al., 2020; Johnson et al., 2021).

6 Conclusions

Long-term daily stream temperature datasets enabled development of generalized additive models (GAMs) that include nonlinear and seasonally varying effects of flow and air temperature on stream temperature. Cross-validation indicated these models had higher accuracy than models that did not account for seasonally variable effects of flow, providing evidence that flow is important in controlling stream temperatures and that the influence of flow is variable through time. Results from these models indicated that high river flow had a strong cooling effect on river temperatures during April through July at 10 sites in the Klamath Basin of California, corroborating similar findings from western North America.

Results from extrapolation cross-validation tests show that our selected model is robust in estimating stream temperatures under environmental conditions moderately outside of the range of conditions used to train the model (although see cautions in Section 5.5). We applied the model to instream flow management scenarios proposed by regulatory agencies at our focal study site, the Scott River, finding that these scenarios would improve stream temperatures. Relative to historic conditions, the higher instream flow scenario would reduce annual maximum temperature from 25.2 °C to 24.1 °C, reduce annual exceedances of 22 °C (a cumulative thermal stress metric) from 106 to 51 degree-days, and delay onset of water temperatures >22 °C during some drought years.

These models contribute to an emerging body of work demonstrating the use of GAMs for predicting daily river temperatures. Our models are easy to implement and improve prediction accuracy of stream temperature responses to flow changes over models without seasonally variable effects of flow, providing tools that managers can use to select flow solutions most likely to protect species and ecosystems. The models are implemented in the R software environment with publicly accessible code. Testing at 10 streams in our study region indicated that models with seasonally variable flow effects had high prediction accuracy across all streams, suggesting that these models have broad applicability over a range of stream types. Our selected model, GAM7, incrementally improves upon previous methods for representing flow effects. Model applications include those explored here (i.e., scenario prediction and identifying periods of flow importance), as well as filling gaps in temperature time series. We suggest that GAM7, as well as similar model structures (i.e., GAM6, GAM8) will perform well across a range of streams. Model validation procedures, including extrapolation-based methods when models are applied to new data, should be conducted to test model accuracy at new sites and for datasets of variable periods of record.

CRediT authorship contribution statement

J.E.A.: Conceptualization, Data curation, Methodology, Formal analysis, Visualization, Writing – original draft, Writing – review & editing. C.R.: Conceptualization, Investigation, Data curation, Funding acquisition, Project administration, Writing - review & editing. L.G.: Writing - review & editing.

Acknowledgments

The Klamath Tribal Water Quality Consortium (Karuk Tribe, Yurok Tribe, Hoopa Valley Tribe, Quartz Valley Indian Reservation, and Resighini Rancheria) supported J.E.A. and L.G. using funds provided by the U.S. Environmental Protection Agency, Region 9. Maija Meneks (KNF) and Callie McConnell (USFS Corvallis) provided the USFS water temperature data. Isaiah Williams, Alex Case, Sean Ryan and Marla Bennett (QVIR) assisted with data collection. Taylor Daley (USFWS Arcata) provided USFWS water temperature data. Daniel Isaak and Sara John provided data from Isaak et al. (2018) and FitzGerald et al. (2021), respectively. WRR editors and reviewers provided comments that substantially improved this manuscript.

Data Availability Statement

All input and output data and codes are archived in the online repository HydroShare (Asarian et al., 2023, https://doi.org/10.4211/hs.a6653e2919964f9b840ec0340d86e11c). USBR and USGS stream temperature data (Smith et al., 2018) are also available at https://or.water.usgs.gov/cgi-bin/grapher/graph_setup.pl?site_id=11519500 and https://cdec.water.ca.gov/dynamicapp/staMeta?station_id=RCL. CDWR stream temperature data are also available are available at https://wdl.water.ca.gov/WaterDataLibrary/StationDetails.aspx?Station=F3410000. Gridded PRISM air temperature data (Daly et al., 2008) are also available at: https://prism.oregonstate.edu/explorer/.

References

Alger, M., Lane, B. A., & Neilson, B. T. (2021). Combined influences of irrigation diversions and associated subsurface return flows on river temperature in a semi-arid region. *Hydrological Processes*, 35(8), e14283. https://doi.org/10.1002/hyp.14283

Amodio, S., Aria, M., & D'Ambrosio, A. (2014). On concurvity in nonlinear and nonparametric regression models. *Statistica*, 74(1), 85–98. https://doi.org/10.6092/issn.1973-2201/4599

Arismendi, I., Safeeq, M., Dunham, J. B., & Johnson, S. L. (2014). Can air temperature be used to project influences of climate change on stream temperature? *Environmental Research Letters*, 9(8), 084015. https://doi.org/10.1088/1748-9326/9/8/084015

Arora, R., Tockner, K., & Venohr, M. (2016). Changing river temperatures in northern Germany: Trends and drivers of change. *Hydrological Processes*, 30(17), 3084–3096. https://doi.org/10.1002/hyp.10849

Asarian, J.E., Cressey, L., Bennett, B., Grunbaum, J., Cyr, L., Soto, T., & Robinson, C. (2020). Influence of snowpack, streamflow, air temperature, and wildfire smoke on Klamath Basin stream temperatures, 1995-2017. Eureka, CA: Riverbend Sciences. https://doi.org/10.13140/RG.2.2.22934.47681

Asarian, J. E., Robinson, C., & Genzoli, L. (2023). Data and codes for: Modeling seasonal effects of river flow on water temperatures in an agriculturally dominated California river [Dataset]. HydroShare, https://doi.org/10.4211/hs.a6653e2919964f9b840ec0340d86e11c

Asarian, J. E., & Walker, J. D. (2016). Long-term trends in streamflow and precipitation in Northwest California and Southwest Oregon, 1953-2012. *Journal of the American Water Resources Association*, 52(1), 241–261. https://doi.org/10.1111/1752-1688.12381

Baayen, R. H., van Rij, J., de Cat, C., & Wood, S. (2018). Autocorrelated errors in experimental data in the language sciences: some solutions offered by generalized additive mixed models. In D. Speelman, K. Heylen, & D. Geeraerts (Eds.), *Mixed-Effects Regression Models in Linguistics* (pp. 49–69). Springer International Publishing. https://doi.org/10.1007/978-3-319-69830-4_4

Bartholow, J. M. (1991). A modeling assessment of the thermal regime for an urban sport fishery. *Environmental Management*, 15(6), 833. https://doi.org/10.1007/BF02394821

Benyahya, L., Caissie, D., St-Hilaire, A., Ouarda, T. B. M. J., & Bobée, B. (2007a). A review of statistical water temperature models. *Canadian Water Resources Journal / Revue Canadienne Des Ressources Hydriques*, 32(3), 179–192. https://doi.org/10.4296/cwrj3203179

Benyahya, L., St-Hilaire, A., Quarda, T. B. M. J., Bobée, B., & Ahmadi-Nedushan, B. (2007b). Modeling of water temperatures based on stochastic approaches: Case study of the Deschutes River. *Journal of Environmental Engineering and Science*, 6(4), 437–448. https://doi.org/10.1139/s06-067

Benyahya, L., St-Hilaire, A., Ouarda, T., Bobee, B., & Dumas, J. (2008). Comparison of non-parametric and parametric water temperature models on the Nivelle River, France. *Hydrological Sciences Journal*, 53(3), 640–655.

Bogan, T., Mohseni, O., & Stefan, H. G. (2003). Stream temperature-equilibrium temperature relationship. *Water Resources Research*, 39(9), 1245. https://doi.org/10.1029/2003WR002034

Boudreault, J., Bergeron, N. E., St-Hilaire, A., & Chebana, F. (2019). Stream temperature modeling using functional regression models. *Journal of the American Water Resources Association*, 55(6), 1382–1400. https://doi.org/10.1111/1752-1688.12778

Boyd, M., and Kasper, B. (2003). Analytical methods for dynamic open channel heat and mass transfer: Methodology for Heat Source model version 7.0. Portland, OR: Oregon Department of Environmental Quality.

Brewitt, K. S., & Danner, E. M. (2014). Spatio-temporal temperature variation influences juvenile steelhead (*Oncorhynchus mykiss*) use of thermal refuges. *Ecosphere*, 5(7), art92. https://doi.org/10.1890/ES14-00036.1

Briggs, M. A., Johnson, Z. C., Snyder, C. D., Hitt, N. P., Kurylyk, B. L., Lautz, L., Irvine, D. J., Hurley, S. T., & Lane, J. W. (2018). Inferring watershed hydraulics and cold-water habitat persistence using multi-year air and stream temperature signals. *Science of The Total Environment*, 636, 1117–1127. https://doi.org/10.1016/j.scitotenv.2018.04.344

Brown, G. W. (1969). Predicting temperatures of small streams. *Water Resources Research*, 5(1), 68–75. https://doi.org/10.1029/WR005i001p00068

Cade, B. S., & Noon, B. R. (2003). A gentle introduction to quantile regression for ecologists. *Frontiers in Ecology and the Environment*, 1(8), 412–420. https://doi.org/10.1890/1540-9295(2003)001[0412:AGITQR]2.0.CO;2

Caissie, D. (2006). The thermal regime of rivers: A review. *Freshwater Biology*, 51(8), 1389–1406. https://doi.org/10.1111/j.1365-2427.2006.01597.x

Caissie, D., El-Jabi, N., & Satish, M. G. (2001). Modelling of maximum daily water temperatures in a small stream using air temperatures. *Journal of Hydrology*, 251(1), 14–28. https://doi.org/10.1016/S0022-1694(01)00427-9

Caldwell, R. J., Gangopadhyay, S., Bountry, J., Lai, Y., & Elsner, M. M. (2013). Statistical modeling of daily and subdaily stream temperatures: Application to the Methow River Basin, Washington. *Water Resources Research*, 49(7), 4346–4361. https://doi.org/10.1002/wrcr.20353

CDFW (California Department of Fish and Wildlife) (2017). Interim Instream Flow Criteria for the Protection of Fishery Resources in the Scott River Watershed, Siskiyou County. https://web.archive.org/web/20210324204650if_/https://nrm.dfg.ca.gov/FileHandler.ashx?DocumentID=143476.

Chandesris, A., Van Looy, K., Diamond, J. S., & Souchon, Y. (2019). Small dams alter thermal regimes of downstream water. *Hydrology and Earth System Sciences*, 23(11), 4509–4525. https://doi.org/10.5194/hess-23-4509-2019

Cline, T. J., Schindler, D. E., Walsworth, T. E., French, D. W., & Lisi, P. J. (2020). Low snowpack reduces thermal response diversity among streams across a landscape. *Limnology and Oceanography Letters*, 5(3), 254–263. https://doi.org/10.1002/lol2.10148.

Coleman, D., Bevitt, R., & Reinfelds, I. (2021). Predicting the thermal regime change of a regulated snowmelt river using a generalised additive model and analogue reference streams. *Environmental Processes*, 8(2), 511–531. https://doi.org/10.1007/s40710-021-00501-7

Crozier, L. G., Siegel, J. E., Wiesebron, L. E., Trujillo, E. M., Burke, B. J., Sandford, B. P., & Widener, D. L. (2020). Snake River sockeye and Chinook salmon in a changing climate: Implications for upstream migration survival during recent extreme and future climates. *PLOS ONE*, 15(9), e0238886. https://doi.org/10.1371/journal.pone.0238886

Dahlke, H., Brown, A., Orloff, S., Putnam, D., & O'Geen, T. (2018). Managed winter flooding of alfalfa recharges groundwater with minimal crop damage. *California Agriculture*, 72(1), 1–11. https://doi.org/10.3733/ca.2018a0001

Daly, C., Halbleib, M., Smith, J. I., Gibson, W. P., Doggett, M. K., Taylor, G. H., Curtis, J., & Pasteris, P. P. (2008). Physiographically sensitive mapping of climatological temperature and precipitation across the conterminous United States. *International Journal of Climatology*, 28(15), 2031–2064. https://doi.org/10.1002/joc.1688

David, A. T., Asarian, J. E., & Lake, F. K. (2018). Wildfire smoke cools summer river and stream water temperatures. *Water Resources Research*, 54(10), 7273–7290. https://doi.org/10.1029/2018WR022964

Drake, D., Tate, K., & Carlson, H. (2000). Analysis shows climate-caused decreases in Scott River fall flows. *California Agriculture*, 54(6), 46–49. https://doi.org/10.3733/ca.v054n06p46

Dugdale, S. J., Hannah, D. M., & Malcolm, I. A. (2017). River temperature modelling: A review of process-based approaches and future directions. *Earth-Science Reviews*, 175, 97–113. https://doi.org/10.1016/j.earscirev.2017.10.009

Dugdale, S. J., Malcolm, I. A., Kantola, K., & Hannah, D. M. (2018). Stream temperature under contrasting riparian forest cover: Understanding thermal dynamics and heat exchange processes. *Science of The Total Environment*, 610–611, 1375–1389. https://doi.org/10.1016/j.scitotenv.2017.08.198

Dunham, J., Chandler, G., Rieman, B., Martin, D. (2005). Measuring stream temperature with digital data loggers: A user's guide (*USDA Forest Service Gen. Tech. Rep.* RMRSGTR-150WWW). http://www.fs.fed.us/rm/pubs/rmrs_gtr150.pdf

Dymond, J. R. (1984). Water temperature change caused by abstraction. *Journal of Hydraulic Engineering*, 110(7), 987–991. https://doi.org/10.1061/(ASCE)0733-9429(1984)110:7(987)

Fasiolo, M., Wood, S. N., Zaffran, M., Nedellec, R., & Goude, Y. (2020). Fast calibrated additive quantile regression. *Journal of the American Statistical Association*, 1–11. https://doi.org/10.1080/01621459.2020.1725521

Ficklin, D. L., Barnhart, B. L., Knouft, J. H., Stewart, I. T., Maurer, E. P., Letsinger, S. L., & Whittaker, G. W. (2014). Climate change and stream temperature projections in the Columbia River basin: Habitat implications of spatial variation in hydrologic drivers. *Hydrology and Earth System Sciences*, 18(12), 4897–4912. https://doi.org/10.5194/hess-18-4897-2014

FitzGerald, A. M., John, S. N., Apgar, T. M., Mantua, N. J., & Martin, B. T. (2021). Quantifying thermal exposure for migratory riverine species: Phenology of Chinook salmon populations predicts thermal stress. *Global Change Biology*, 27(3), 536–549. https://doi.org/10.1111/gcb.15450

Foglia, L., McNally, A., & Harter, T. (2013). Coupling a spatiotemporally distributed soil water budget with stream-depletion functions to inform stakeholder-driven management of groundwater-dependent ecosystems. *Water Resources Research*, 49(11), 7292–7310. https://doi.org/10.1002/wrcr.20555

Foglia, L., Neumann, J., Tolley, D., Orloff, S., Snyder, R., & Harter, T. (2018). Modeling guides groundwater management in a basin with river–aquifer interactions. *California Agriculture*, 72(1), 84–95. https://doi.org/10.3733/ca.2018a0011

Folegot, S., Hannah, D. M., Dugdale, S. J., Kurz, M. J., Drummond, J. D., Klaar, M. J., Lee-Cullin, J., Keller, T., Martí, E., Zarnetske, J. P., Ward, A. S., & Krause, S. (2018). Low flow controls on stream thermal dynamics. *Limnologica*, 68, 157–167. https://doi.org/10.1016/j.limno.2017.08.003

Fullerton, A. H., Torgersen, C. E., Lawler, J. J., Faux, R. N., Steel, E. A., Beechie, T. J., Ebersole, J. L., & Leibowitz, S. G. (2015). Rethinking the longitudinal stream temperature paradigm: Region-wide comparison of thermal infrared imagery reveals unexpected complexity of river temperatures. *Hydrological Processes*, 29(22), 4719–4737. https://doi.org/10.1002/hyp.10506

Gibeau, P., & Palen, W. J. (2020). Predicted effects of flow diversion by run-of-river hydropower on bypassed stream temperature and bioenergetics of salmonid fishes. *River Research and Applications*, 36(9), 1903–1915. https://doi.org/10.1002/rra.3706

Georges, B., Michez, A., Latte, N., Lejeune, P., & Brostaux, Y. (2021). Water stream heating dynamics around extreme temperature events: An innovative method combining GAM and differential equations. *Journal of Hydrology*, 601, 126600. https://doi.org/10.1016/j.jhydrol.2021.126600

Glover, R. S., Soulsby, C., Fryer, R. J., Birkel, C., & Malcolm, I. A. (2020). Quantifying the relative importance of stock level, river temperature and discharge on the abundance of juvenile Atlantic salmon (*Salmo salar*). *Ecohydrology*, 13(6), e2231. https://doi.org/10.1002/eco.2231

Gu, R. R., & Li, Y. (2002). River temperature sensitivity to hydraulic and meteorological parameters. *Journal of Environmental Management*, 66(1), 43–56. https://doi.org/10.1006/jema.2002.0565

Gu, R., Montgomery, S., & Austin, T. A. (1998). Quantifying the effects of stream discharge on summer river temperature. *Hydrological Sciences Journal*, 43(6), 885–904. https://doi.org/10.1080/02626669809492185

Hannah, D. M., Malcolm, I. A., & Bradley, C. (2009). Seasonal hyporheic temperature dynamics over riffle bedforms. *Hydrological Processes*, 23(15), 2178–2194. https://doi.org/10.1002/hyp.7256

Imholt, C., Gibbins, C. N., Malcolm, I. A., Langan, S., & Soulsby, C. (2010). Influence of riparian cover on stream temperatures and the growth of the mayfly *Baetis rhodani* in an upland stream. *Aquatic Ecology*, 44(4), 669–678. https://doi.org/10.1007/s10452-009-9305-0

Isaak, D. J., Luce, C. H., Horan, D. L., Chandler, G. L., Wollrab, S. P., Dubois, W. B., & Nagel, D. E. (2020). Thermal regimes of perennial rivers and streams in the Western United States. *Journal of the American Water Resources Association*, 1752-1688.12864. https://doi.org/10.1111/1752-1688.12864

Isaak, D. J., Luce, C. H., Horan, D. L., Chandler, G. L., Wollrab, S. P., & Nagel, D. E. (2018). Global warming of salmon and trout rivers in the Northwestern U.S.: Road to ruin or path through purgatory? *Transactions of the American Fisheries Society*, 147(3), 566–587. https://doi.org/10.1002/tafs.10059

Isaak, D. J., Wenger, S. J., Peterson, E. E., Hoef, J. M. V., Nagel, D. E., Luce, C. H., Hostetler, S. W., Dunham, J. B., Roper, B. B., Wollrab, S. P., Chandler, G. L., Horan, D. L., & Parkes-Payne, S. (2017). The NorWeST summer stream temperature model and scenarios for the Western U.S.: A crowd-sourced database and new geospatial tools foster a user community and predict broad climate warming of rivers and streams. *Water Resources Research*, 53(11), 9181–9205. https://doi.org/10.1002/2017WR020969

Islam, S. U., Hay, R. W., Déry, S. J., & Booth, B. P. (2019). Modelling the impacts of climate change on riverine thermal regimes in western Canada's largest Pacific watershed. *Scientific Reports*, 9, 11398. https://doi.org/10.1038/s41598-019-47804-2

Jackson, F. L., Fryer, R. J., Hannah, D. M., Millar, C. P., & Malcolm, I. A. (2018). A spatio-temporal statistical model of maximum daily river temperatures to inform the management of Scotland's Atlantic salmon rivers under climate change. *Science of The Total Environment*, 612, 1543–1558. https://doi.org/10.1016/j.scitotenv.2017.09.010

Johnson, S. L. (2004). Factors influencing stream temperatures in small streams: Substrate effects and a shading experiment. *Canadian Journal of Fisheries and Aquatic Sciences*, 61(6), 913–923.

Johnson, Z. C., Johnson, B. G., Briggs, M. A., Snyder, C. D., Hitt, N. P., & Devine, W. D. (2021). Heed the data gap: Guidelines for using incomplete datasets in annual stream temperature analyses. *Ecological Indicators*, 122, 107229. https://doi.org/10.1016/j.ecolind.2020.107229

Kelleher, C., Wagener, T., Gooseff, M., McGlynn, B., McGuire, K., & Marshall, L. (2012). Investigating controls on the thermal sensitivity of Pennsylvania streams. *Hydrological Processes*, 26(5), 771–785. https://doi.org/10.1002/hyp.8186

Kim, J.-S., & Jain, S. (2010). High-resolution streamflow trend analysis applicable to annual decision calendars: A western United States case study. *Climatic Change*, 102(3–4), 699–707. https://doi.org/10.1007/s10584-010-9933-3

KNF (Klamath National Forest) (2010). Klamath National Forest Sediment and Temperature Monitoring Plan and Quality Assurance Project Plan. Yreka, CA: Klamath National Forest. https://web.archive.org/web/http://www.waterboards.ca.gov/water_issues/programs/tmdl/records/region_1/2013/ref4082.pdf.

KNF (Klamath National Forest) (2011). Klamath National Forest, Water and Air Temperature Monitoring Protocol, May 2011. Yreka, CA: Klamath National Forest.

Klemeš, V. (1986). Operational testing of hydrological simulation models. *Hydrological Sciences Journal*, 31(1), 13–24. https://doi.org/10.1080/02626668609491024

Klos, P. Z., Link, T. E., & Abatzoglou, J. T. (2014). Extent of the rain-snow transition zone in the western U.S. under historic and projected climate. *Geophysical Research Letters*, 41(13), 4560–4568. https://doi.org/10.1002/2014GL060500

Koch, H., & Grünewald, U. (2010). Regression models for daily stream temperature simulation: Case studies for the river Elbe, Germany. *Hydrological Processes*, 24(26), 3826–3836. https://doi.org/10.1002/hyp.7814

Kurylyk, B. L., MacQuarrie, K. T. B., Linnansaari, T., Cunjak, R. A., & Curry, R. A. (2015). Preserving, augmenting, and creating cold-water thermal refugia in rivers: Concepts derived from research on the Miramichi River, New Brunswick (Canada). *Ecohydrology*, 8(6), 1095–1108. https://doi.org/10.1002/eco.1566

Laanaya, F., St-Hilaire, A., & Gloaguen, E. (2017). Water temperature modelling: Comparison between the generalized additive model, logistic, residuals regression and linear regression models. *Hydrological Sciences Journal*, 62(7), 1078–1093. https://doi.org/10.1080/02626667.2016.1246799

Leach, J. A., & Moore, R. D. (2019). Empirical stream thermal sensitivities may underestimate stream temperature response to climate warming. *Water Resources Research*, 55(7), 5453–5467. https://doi.org/10.1029/2018WR024236

Lee, S.-Y., Fullerton, A. H., Sun, N., & Torgersen, C. E. (2020). Projecting spatiotemporally explicit effects of climate change on stream temperature: A model comparison and implications for coldwater fishes. *Journal of Hydrology*, 588, 125066. https://doi.org/10.1016/j.jhydrol.2020.125066

Letcher, B. H., Hocking, D. J., O'Neil, K., Whiteley, A. R., Nislow, K. H., & O'Donnell, M. J. (2016). A hierarchical model of daily stream temperature using air-water temperature synchronization, autocorrelation, and time lags. *PeerJ*, 4, e1727. https://doi.org/10.7717/peerj.1727

Li, H., Deng, X., Kim, D.-Y., & Smith, E. P. (2014). Modeling maximum daily temperature using a varying coefficient regression model. *Water Resources Research*, 50(4), 3073–3087. https://doi.org/10.1002/2013WR014243

Luce, C., Staab, B., Kramer, M., Wenger, S., Isaak, D., & McConnell, C. (2014). Sensitivity of summer stream temperatures to climate variability in the Pacific Northwest. *Water Resources Research*, 50(4), 3428–3443. https://doi.org/10.1002/2013WR014329

Luo, Y., Ficklin, D. L., Liu, X., & Zhang, M. (2013). Assessment of climate change impacts on hydrology and water quality with a watershed modeling approach. *Science of The Total Environment*, 450–451, 72–82. https://doi.org/10.1016/j.scitotenv.2013.02.004

Lute, A. C., & Luce, C. H. (2017). Are model transferability and complexity antithetical? Insights from validation of a variable-complexity empirical snow model in space and time. *Water Resources Research*, 53(11), 8825–8850. https://doi.org/10.1002/2017WR020752

Manhard, C. V., N. A. Som, E. C. Jones, & R. W. Perry. 2018. Estimation of stream conditions in tributaries of the Klamath River, Northern California (*Arcata Fisheries Technical Report* Number TR 2018-32). Arcata, CA: U.S. Fish and Wildlife Service. https://web.archive.org/web/https://www.fws.gov/arcata/fisheries/reports/technical/2018/EstimationofStreamConditionsinTributariesoftheKlamathRiverNorthernCalifornia.pdf

Mayer, T. D. (2012). Controls of summer stream temperature in the Pacific Northwest. *Journal of Hydrology*, 475(0), 323–335. https://doi.org/10.1016/j.jhydrol.2012.10.012

Meier, W., Bonjour, C., Wüest, A., & Reichert, P. (2003). Modeling the effect of water diversion on the temperature of mountain streams. *Journal of Environmental Engineering*, 129(8), 755–764. https://doi.org/10.1061/(ASCE)0733-9372(2003)129:8(755)

Mierau, D. W., Trush, W. J., Rossi, G. J., Carah, J. K., Clifford, M. O., & Howard, J. K. (2017). Managing diversions in unregulated streams using a modified percent-of-flow approach. *Freshwater Biology*. https://doi.org/10.1111/fwb.12985

Mohseni, O., & Stefan, H. G. (1999). Stream temperature/air temperature relationship: A physical interpretation. *Journal of Hydrology*, 218(3), 128–141. https://doi.org/10.1016/S0022-1694(99)00034-7

Mohseni, O., Stefan, H. G., & Erickson, T. R. (1998). A nonlinear regression model for weekly stream temperatures. *Water Resources Research*, 34(10), 2685–2692. https://doi.org/10.1029/98WR01877

Moore, R. D., Spittlehouse, D. L., & Story, A. (2005). Riparian microclimate and stream temperature response to forest harvesting: A review. *Journal of the American Water Resources Association*, 41(4), 813–834. https://doi.org/10.1111/j.1752-1688.2005.tb03772.x

Neumann David W., Rajagopalan Balaji, & Zagona Edith A. (2003). Regression model for daily maximum stream temperature. *Journal of Environmental Engineering*, 129(7), 667–674. https://doi.org/10.1061/(ASCE)0733-9372(2003)129:7(667)

Nichols, A. L., Willis, A. D., Jeffres, C. A., & Deas, M. L. (2014). Water temperature patterns below large groundwater springs: management implications for coho salmon in the Shasta River, California. *River Research and Applications*, 30(4), 442–455. https://doi.org/10.1002/rra.2655

NCRWQCB (North Coast Regional Water Quality Control Board) (2005). *Staff Report for the Action Plan for the Scott River Watershed Sediment and Temperature Total Maximum Daily Loads*. Santa Rosa, CA: North Coast Regional Water Quality Control Board. https://www.waterboards.ca.gov/northcoast/water_issues/programs/tmdls/scott_river/staff_report

Null, S. E., Mouzon, N. R., & Elmore, L. R. (2017). Dissolved oxygen, stream temperature, and fish habitat response to environmental water purchases. *Journal of Environmental Management*, 197, 559–570. https://doi.org/10.1016/j.jenvman.2017.04.016

Null, S. E., Viers, J. H., Deas, M. L., Tanaka, S. K., & Mount, J. F. (2013). Stream temperature sensitivity to climate warming in California's Sierra Nevada: Impacts to coldwater habitat. *Climatic Change*, 116(1), 149–170. https://doi.org/10.1007/s10584-012-0459-8

Ouellet, V., St-Hilaire, A., Dugdale, S. J., Hannah, D. M., Krause, S., & Proulx-Ouellet, S. (2020). River temperature research and practice: Recent challenges and emerging opportunities for managing thermal habitat conditions in stream ecosystems. *Science of The Total Environment*, 736, 139679. https://doi.org/10.1016/j.scitotenv.2020.139679

Pedersen, E. J., Miller, D. L., Simpson, G. L., & Ross, N. (2019). Hierarchical generalized additive models in ecology: An introduction with mgcv. *PeerJ*, 7, e6876. https://doi.org/10.7717/peerj.6876

Persad, G. G., Swain, D. L., Kouba, C., & Ortiz-Partida, J. P. (2020). Inter-model agreement on projected shifts in California hydroclimate characteristics critical to water management. *Climatic Change*. https://doi.org/10.1007/s10584-020-02882-4

Piotrowski, A. P., & Napiorkowski, J. J. (2019). Simple modifications of the nonlinear regression stream temperature model for daily data. *Journal of Hydrology*, 572, 308–328. https://doi.org/10.1016/j.jhydrol.2019.02.035

Poff, N. L., Tharme, R. E., & Arthington, A. H. (2017). Evolution of environmental flows assessment science, principles, and methodologies. In A. C. Horne, J. A. Webb, M. J. Stewardson, B. Richter, & M. Acreman (Eds.), *Water for the Environment* (pp. 203–236). Academic Press. https://doi.org/10.1016/B978-0-12-803907-6.00011-5

QVIR (Quartz Valley Indian Reservation) (2016). Quality assurance project plan 2016 revision water quality sampling and analysis, CWA 106 grant identification # I-96927206-0. Fort Jones, CA: QVIR Tribal Environmental Protection Department.

Railsback, S. F., Harvey, B. C., Kupferberg, S. J., Lang, M. M., McBain, S., & Welsh, H. H. (2016). Modeling potential river management conflicts between frogs and salmonids. *Canadian Journal of Fisheries and Aquatic Sciences*, 73(5), 773–784. https://doi.org/10.1139/cjfas-2015-0267

Roberts, D. R., Bahn, V., Ciuti, S., Boyce, M. S., Elith, J., Guillera-Arroita, G., Hauenstein, S., Lahoz-Monfort, J. J., Schröder, B., Thuiller, W., Warton, D. I., Wintle, B. A., Hartig, F., & Dormann, C. F. (2017). Cross-validation strategies for data with temporal, spatial, hierarchical, or phylogenetic structure. *Ecography*, 40(8), 913–929. https://doi.org/10.1111/ecog.02881

Romberger, C. Z. and S. Gwozdz (2018). Performance of water temperature management on the Klamath and Trinity Rivers, 2017. (*U.S. Fish and Wildlife Service, Arcata Fisheries Data Series Number DS 2018-59*).

Santiago, J. M., Muñoz-Mas, R., Solana-Gutiérrez, J., García de Jalón, D., Alonso, C., Martínez-Capel, F., Pórtoles, J., Monjo, R., & Ribalaygua, J. (2017). Waning habitats due to climate change: The effects of changes in streamflow and temperature at the rear edge of the distribution of a cold-water fish. *Hydrology and Earth System Sciences*, 21(8), 4073–4101. https://doi.org/10.5194/hess-21-4073-2017

Shaw, S. B. (2017). Does an upper limit to river water temperature apply in all places? *Hydrological Processes*, 31(21), 3729–3739. https://doi.org/10.1002/hyp.11297

Siegel, J. E., & Volk, C. J. (2019). Accurate spatiotemporal predictions of daily stream temperature from statistical models accounting for interactions between climate and landscape. *PeerJ*, 7, e7892. https://doi.org/10.7717/peerj.7892

Sinokrot, B. A., & Gulliver, J. S. (2000). In-stream flow impact on river water temperatures. *Journal of Hydraulic Research*, 38(5), 339–349. https://doi.org/10.1080/00221680009498315

Sohrabi, M. M., Benjankar, R., Tonina, D., Wenger, S. J., & Isaak, D. J. (2017). Estimation of daily stream water temperatures with a Bayesian regression approach. *Hydrological Processes*, 31(9), 1719–1733. https://doi.org/10.1002/hyp.11139

Smith, C. D., Rounds, S. A., & Orzol, L. L. (2018). Klamath River Basin water-quality data. (USGS Numbered Series *Fact Sheet* 2018–3031). https://doi.org/10.3133/fs20183031

Soto, B. (2016). Assessment of Trends in Stream Temperatures in the North of the Iberian Peninsula Using a Nonlinear Regression Model for the Period 1950–2013. *River Research and Applications*, 32(6), 1355–1364. https://doi.org/10.1002/rra.2971

Stanford, J.A. & Ward, J.V. (1992). Management of aquatic resources in large catchments: Recognizing interactions between ecosystem connectivity and environmental disturbance. In R. J. Naiman (Editor). *Watershed Management: Balancing Sustainability and Environmental Change* (pp. 91–124). New York, NY: Springer.

Siegel, J. E., Fullerton, A. H., & Jordan, C. E. (2022). Accounting for snowpack and time-varying lags in statistical models of stream temperature. *Journal of Hydrology X*, 17, 100136. https://doi.org/10.1016/j.hydroa.2022.100136

St-Hilaire, A., Boyer, C., Bergeron, N., & Daigle, A. (2018). Water temperature monitoring in Eastern Canada: A case study for network optimization. *WIT Transactions on Ecology and the Environment*, 228, 269–275. https://doi.org/10.2495/WP180251

Steel, E. A., Beechie, T. J., Torgersen, C. E., & Fullerton, A. H. (2017). Envisioning, quantifying, and managing thermal regimes on river networks. *BioScience*, 67(6), 506–522. https://doi.org/10.1093/biosci/bix047

Superior Court of Siskiyou County (1980). Scott River adjudication, decree no. 30662. Scott River stream system, Siskiyou County. Sacramento, CA: State Water Resources Control Board.

Sutton, R. J., Deas, M. L., Tanaka, S. K., Soto, T., & Corum, R. A. (2007). Salmonid observations at a Klamath River thermal refuge under various hydrological and meteorological conditions. *River Research and Applications*, 23(7), 775–785.

Sutton, R., & Soto, T. (2012). Juvenile coho salmon behavioural characteristics in Klamath river summer thermal refugia. *River Research and Applications*. https://doi.org/10.1002/rra.1459

Tague, C., Farrell, M., Grant, G., Lewis, S., & Rey, S. (2007). Hydrogeologic controls on summer stream temperatures in the McKenzie River basin, Oregon. *Hydrological Processes*, 21(24), 3288–3300. https://doi.org/10.1002/hyp.6538

Theurer, F.D., Voos, K.A., & Miller, W.J. (1984). Instream water temperature model. *Instream Flow Information Paper 16*. FWS/OBS-84/15. Washington, D.C.: US Fish and Wildlife Service.

Tolley, D., Foglia, L., & Harter, T. (2019). Sensitivity analysis and calibration of an integrated hydrologic model in an irrigated agricultural basin with a groundwater-dependent ecosystem. *Water Resources Research*, 55(9), 7876–7901. https://doi.org/10.1029/2018WR024209

USEPA (U.S. Environmental Protection Agency) (2003). EPA Region 10 guidance for Pacific Northwest state and tribal temperature water quality standards. EPA 910-B-03-002. Seattle, WA: Region 10 Office of Water.

Van Kirk, R. W., & Naman, S. W. (2008). Relative effects of climate and water use on base-flow trends in the Lower Klamath Basin. *Journal of the American Water Resources Association*, 44(4), 1035–1052. https://doi.org/10.1111/j.1752-1688.2008.00212.x

VanderKooi, S., Thorsteinson, L., & Clark, M. (2011). Environmental and historical setting. In L. Thorsteinson, S. VanderKooi, & W. Duffy (Eds.), *Proceedings of the Klamath Basin Science Conference*, Medford, Oregon, February 1–5, 2010 (pp. 31–36). Reston, VA: U.S. Geological Survey.

van Rij, J., Hendriks, P., van Rijn, H., Baayen, R. H., & Wood, S. N. (2019). Analyzing the time course of pupillometric data. *Trends in Hearing*, 23, 233121651983248. https://doi.org/10.1177/2331216519832483

van Rij, J., Wieling, M., Baayen, R., van Rijn, H. (2020). itsadug: Interpreting time series and autocorrelated data using GAMMs. *R package version 2.4*. https://cran.r-project.org/package=itsadug

van Vliet, M. T. H., Ludwig, F., Zwolsman, J. J. G., Weedon, G. P., & Kabat, P. (2011). Global river temperatures and sensitivity to atmospheric warming and changes in river flow. *Water Resources Research*, 47(2). https://doi.org/10.1029/2010WR009198

Webb, B. W., Clack, P. D., & Walling, D. E. (2003). Water–air temperature relationships in a Devon river system and the role of flow. *Hydrological Processes*, 17(15), 3069–3084. https://doi.org/10.1002/hyp.1280

Webb, B. W., Hannah, D. M., Moore, R. D., Brown, L. E., & Nobilis, F. (2008). Recent advances in stream and river temperature research. *Hydrological Processes*, 22(7), 902–918. https://doi.org/10.1002/hyp.6994

Wenger, S. J., Isaak, D. J., Luce, C. H., Neville, H. M., Fausch, K. D., Dunham, J. B., Dauwalter, D. C., Young, M. K., Elsner, M. M., Rieman, B. E., Hamlet, A. F., & Williams, J. E. (2011). Flow regime, temperature, and biotic interactions drive differential declines of trout species under climate change. *Proceedings of the National Academy of Sciences*, 108(34), 14175–14180. https://doi.org/10.1073/pnas.1103097108

Westerling, A. L. (2016). Increasing western US forest wildfire activity: Sensitivity to changes in the timing of spring. *Philosophical Transactions of the Royal Society B: Biological Sciences*, 371(1696), 20150178. https://doi.org/10.1098/rstb.2015.0178

Wood, S.N. (2017). *Generalized additive models: An introduction with R (2nd edition)*. Chapman and Hall/CRC.

Wrzesiński, D., & Graf, R. (2022). Temporal and spatial patterns of the river flow and water temperature relations in Poland. *Journal of Hydrology and Hydromechanics*, 70(1), 12–29. https://doi.org/10.2478/johh-2021-0033

Yan, H., Sun, N., Fullerton, A., & Baerwalde, M. (2021). Greater vulnerability of snowmelt-fed river thermal regimes to a warming climate. *Environmental Research Letters*, 16(5), 054006. https://doi.org/10.1088/1748-9326/abf393

Yang, G., & Moyer, D. L. (2020). Estimation of nonlinear water-quality trends in high-frequency monitoring data. *Science of The Total Environment*, 715, 136686. https://doi.org/10.1016/j.scitotenv.2020.136686

Yard, M. D., Bennett, G. E., Mietz, S. N., Coggins, L. G., Stevens, L. E., Hueftle, S., & Blinn, D. W. (2005). Influence of topographic complexity on solar insolation estimates for the Colorado River, Grand Canyon, AZ. *Ecological Modelling*, 183(2), 157–172. https://doi.org/10.1016/j.ecolmodel.2004.07.027

Yarnell, S. M., Stein, E. D., Webb, J. A., Grantham, T., Lusardi, R. A., Zimmerman, J., Peek, R. A., Lane, B. A., Howard, J., & Sandoval-Solis, S. (2020). A functional flows approach to selecting ecologically relevant flow metrics for environmental flow applications. *River Research and Applications*, rra.3575. https://doi.org/10.1002/rra.3575

References From the Supporting Information

Daly, C., Doggett, M. K., Smith, J. I., Olson, K. V., Halbleib, M. D., Dimcovic, Z., Keon, D., Loiselle, R. A., Steinberg, B., Ryan, A. D., Pancake, C. M., & Kaspar, E. M. (2021). Challenges in observation-based mapping of daily precipitation across the conterminous United States. *Journal of Atmospheric and Oceanic Technology*, 38(11), 1979–1992. https://doi.org/10.1175/JTECH-D-21-0054.1

Lusardi, R. A., Hammock, B. G., Jeffres, C. A., Dahlgren, R. A., & Kiernan, J. D. (2019). Oversummer growth and survival of juvenile coho salmon (*Oncorhynchus kisutch*) across a natural gradient of stream water temperature and prey availability: An in situ enclosure experiment. *Canadian Journal of Fisheries and Aquatic Sciences*, 1–12. https://doi.org/10.1139/cjfas-2018-0484

McGrath, E. O., Neumann, N. N., & Nichol, C. F. (2017). A statistical model for managing water temperature in streams with anthropogenic influences. *River Research and Applications*, 33(1), 123–134. https://doi.org/10.1002/rra.3057

Menne, M.J., Durre, I., Korzeniewski, B., McNeal, S., Thomas, K., Yin, X., Anthony, S., Ray, R., Vose, R.S., Gleason, B.E., & Houston, T.G. (2012a). Global historical climatology network - daily (GHCN-Daily), version 3.26. NOAA National Climatic Data Center. http://doi.org/10.7289/V5D21VHZ. Accessed 2021-01-11

Menne, M. J., Durre, I., Vose, R. S., Gleason, B. E., & Houston, T. G. (2012b). An overview of the global historical climatology network-daily database. *Journal of Atmospheric and Oceanic Technology*, 29(7), 897–910. https://doi.org/10.1175/JTECH-D-11-00103.1

Moore, R. B., & Dewald, T. G. (2016). The road to NHDPlus—Advancements in digital stream networks and associated catchments. *Journal of the American Water Resources Association*, 52(4), 890–900. https://doi.org/10.1111/1752-1688.12389

Steel, E. A., Kennedy, M. C., Cunningham, P. G., & Stanovick, J. S. (2013). Applied statistics in ecology: Common pitfalls and simple solutions. *Ecosphere*, 4(9), art115. https://doi.org/10.1890/ES13-00160.1

Stenhouse, S., Pisano, M., Bean, C., & Chesney, W. (2012). Water temperature thresholds for coho salmon in a spring fed river, Siskiyou County, California. *California Fish and Game*, 98(1), 19–37.

Welsh, H. H., Hodgson, G. R., Harvey, B. C., & Roche, M. F. (2001). Distribution of juvenile coho salmon in relation to water temperatures in tributaries of the Mattole River, California. *North American Journal of Fisheries Management*, 21(3), 464–470. https://doi.org/10.1577/1548-8675(2001)021<0464:DOJCSI>2.0.CO;2

Zillig, K. W., Lusardi, R. A., Moyle, P. B., & Fangue, N. A. (2021). One size does not fit all: Variation in thermal eco-physiology among Pacific salmonids. *Reviews in Fish Biology and Fisheries*. https://doi.org/10.1007/s11160-020-09632-w

Figure 1. Klamath Basin study sites including the Scott River. Source map credits: Esri , NOAA, and USGS.

Figure 2. Time series of (a) daily mean air temperature, (b) daily mean flow, (c) daily maximum stream temperature (T_{max}), and (d) daily mean stream temperature (T_{mean}) at Scott River from 1998–2020.

Figure 3. Inputs to Scott River "quantile air temperature" scenarios representing 15 combinations of (a) three air temperature inputs and (b) five flow inputs that vary by day. Observed values for 1998–2020 are shown as gray lines.

Figure 4. Model formulas and summary of RMSE from extrapolation and LOYO CV tests at 10 Klamath Basin sites applying T_{max} (top panels) and T_{mean} (bottom panels) models to years (LOYO) or flow and air temperature combinations (extrapolation) not used in model calibration. Models are sorted by overall RMSE rank (i.e., mean rank of all 10 sites and both temperature metrics, Table S2). Extrapolation test RMSE values for top eight models in individual site panels are labeled, with asterisk marking lowest RMSE in each panel. Formulas for T_{max} and T_{mean} models are identical, so are only listed once. Key to formulas: D = day of year from 1 (1 January) to 366 (31 December in leap year); Q = daily mean flow; see Section 3.1.2 for key to 'A' air temperature variables; 's()' is a nonlinear function; 's(D, by =)' is a linear interaction that varies smoothly by D; 'te()' is a fully nonlinear tensor product smooth of two or three variable; and 'ti()' is a tensor product interaction. Except GAM11, all models also include an AR1 autocorrelation structure and random effect of year.

Figure 5. Configuration of data blocks used in extrapolation tests for model selection and validation.

Figure 6. Effects of flow (Q) and day of year (D) on predicted values of (a) T_{max} and (b) T_{mean} in Scott River GAM7. Colors and labeled contour lines show predicted temperatures (°C). Underlying gray dots show calibration data.

Figure 7. Modeled Scott River T_{max} and T_{mean} under the 15 "quantile air temperature" scenarios representing combinations of three air temperature inputs (arranged in columns) and three quantile flow inputs and two management flow inputs (shown by color). Observed values for 1998–2020 are shown as gray lines. Selected data values are labeled on 15 June and the first day of March–October. Horizontal dashed line is the salmonid temperature threshold.

Figure 8. Modeled stream temperature differences between lowest flow (0.1 quantile) and highest flow (0.9 quantile) scenarios throughout the year for (a) T_{max} and (b) T_{mean} at 10 Klamath Basin sites estimated using GAM7.

Figure 9. (a) Annual maximum stream temperature, (b) annual degree-days exceeding 22 °C, and (c) first and (d) last day when T_{max} exceeded 22 °C in Scott River model scenarios pairing observed air temperatures with eight flow scenarios. Means of all years are shown with black points and grey "x" show individual years, offset for clarity.

Table 1. Matrix showing model scenarios representing combinations of air temperature and flow inputs, and organized into two scenario groups. The first group (15 scenarios) used "quantile air temperature" inputs (6 were only run only at Scott River while 9 were run at all Klamath Basin sites) and the second group (8 scenarios) were run only at Scott River and used "observed air temperature" inputs.

Scenario group	**Air temperature inputs**	**Flow inputs**							
		Lowest (0.1 quantile)	**Typical** (0.5 quantile)	**Highest** (0.9 quantile)	**USFS water right**	**CDFW flow criteria**	**Observed**	**Maximum of observed or USFS**	**Maximum of observed or CDFW**
Quantile air temperature	**Hottest** (0.9 quantile)	All sites	All sites	All sites	Scott only	Scott only			
	Typical (0.5 quantile)	All sites	All sites	All sites	Scott only	Scott only			
	Coolest (0.1 quantile)	All sites	All sites	All sites	Scott only	Scott only			
Observed air temperature	**Observed** (measured on date)	Scott only	Scott only	Scott only	Scott only	Scott only	Scott only	Scott only	Scott only

Figure 1.

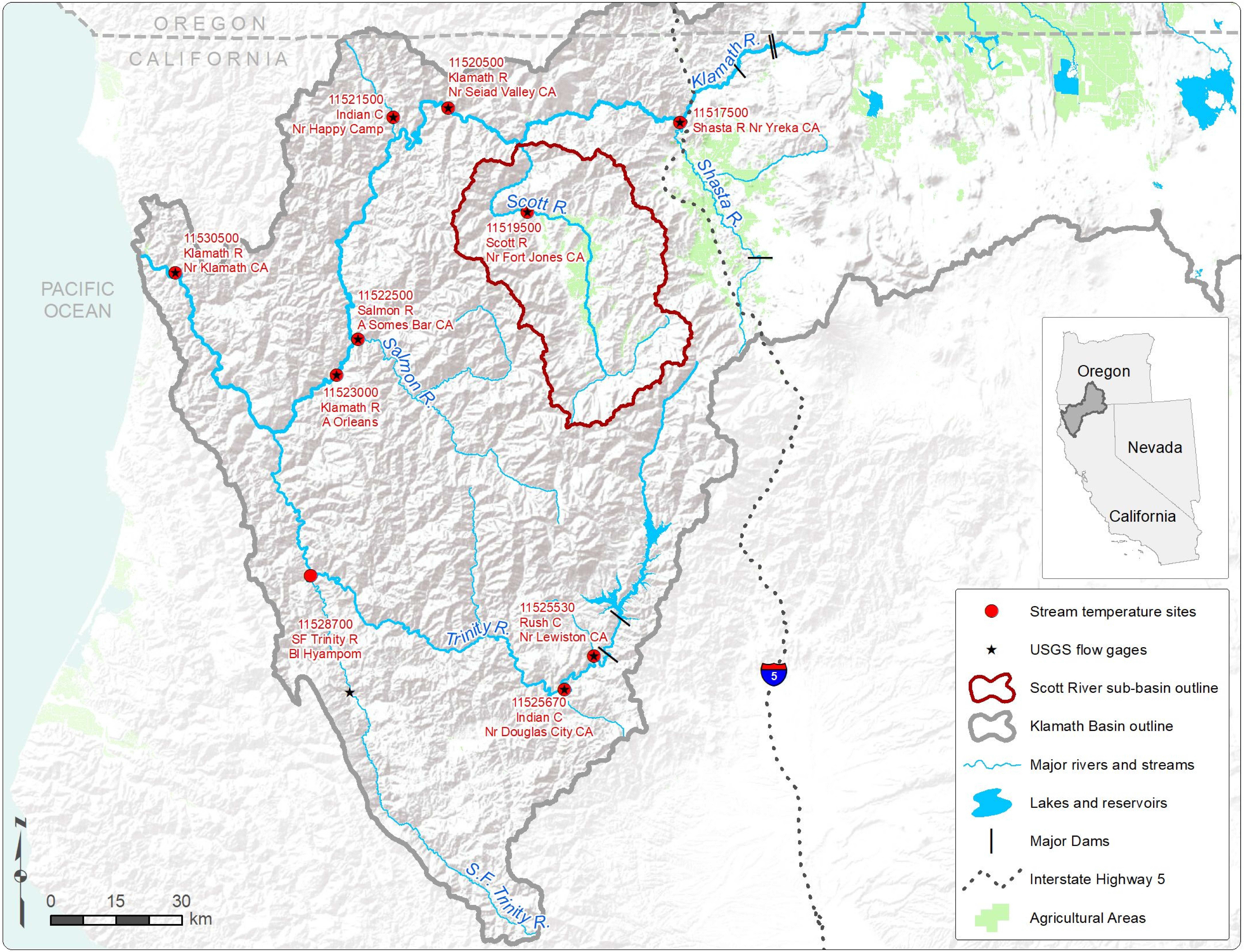

OREGON
CALIFORNIA
PACIFIC OCEAN
11520500 Klamath R Nr Seiad Valley CA
11521500 Indian C Nr Happy Camp
11517500 Shasta R Nr Yreka CA
Klamath R.
Shasta R.
Scott R.
11519500 Scott R Nr Fort Jones CA
11530500 Klamath R Nr Klamath CA
11522500 Salmon R A Somes Bar CA
Salmon R.
11523000 Klamath R A Orleans
11528700 SF Trinity R Bl Hyampom
11525530 Rush C Nr Lewiston CA
Trinity R.
11525670 Indian C Nr Douglas City CA
S.F. Trinity R.
5
Oregon
Nevada
California
Stream temperature sites
USGS flow gages
Scott River sub-basin outline
Klamath Basin outline
Major rivers and streams
Lakes and reservoirs
Major Dams
Interstate Highway 5
Agricultural Areas
N
0 15 30 km

Figure 2.

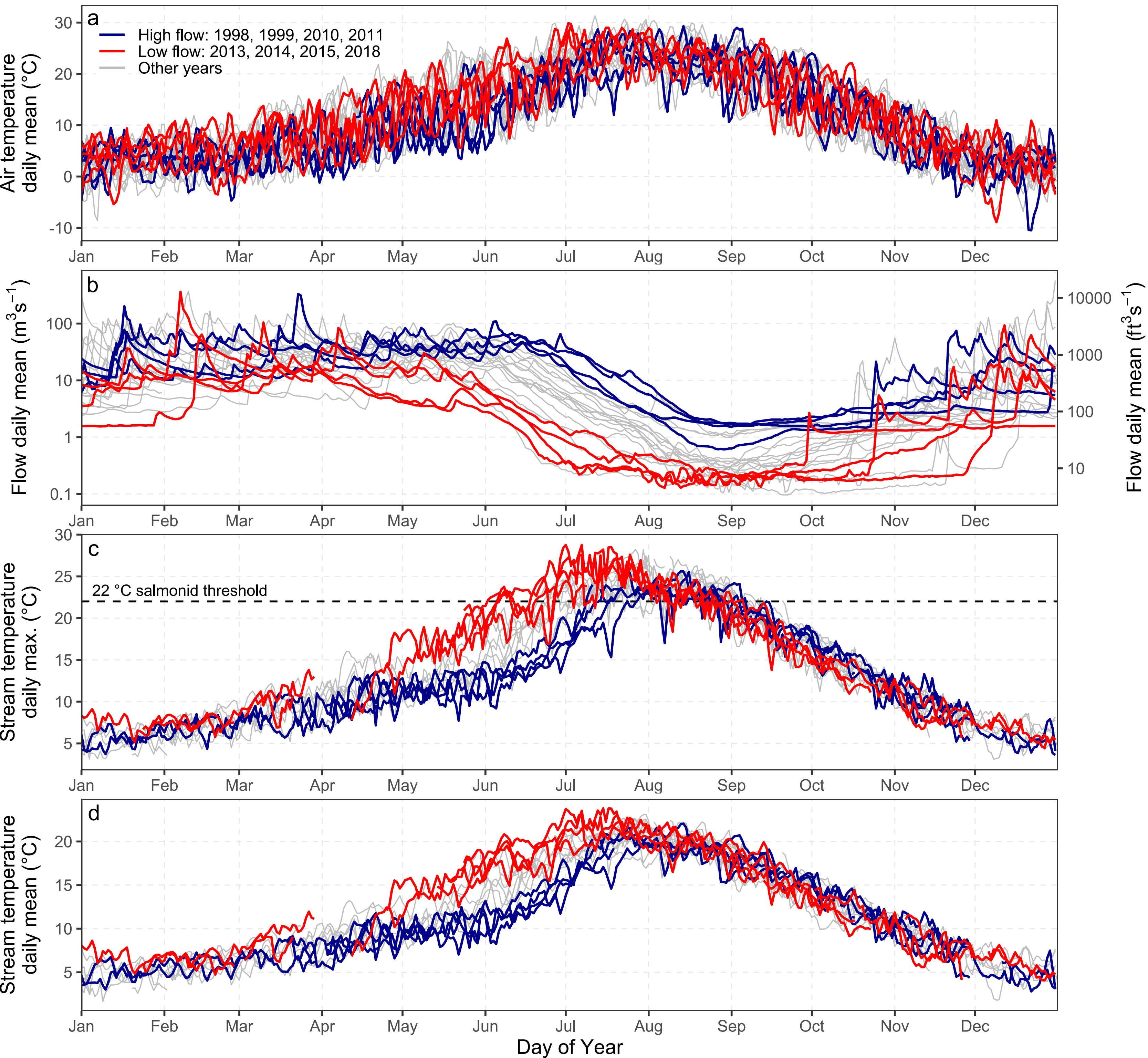
a
High flow: 1998, 1999, 2010, 2011
Low flow: 2013, 2014, 2015, 2018
Other years
Air temperature daily mean (°C)
b
Flow daily mean (m^3s^{-1})
Flow daily mean (ft^3s^{-1})
c
22 °C salmonid threshold
Stream temperature daily max. (°C)
d
Stream temperature daily mean (°C)
Jan
Feb
Mar
Apr
May
Jun
Jul
Aug
Sep
Oct
Nov
Dec
Day of Year

Figure 3.

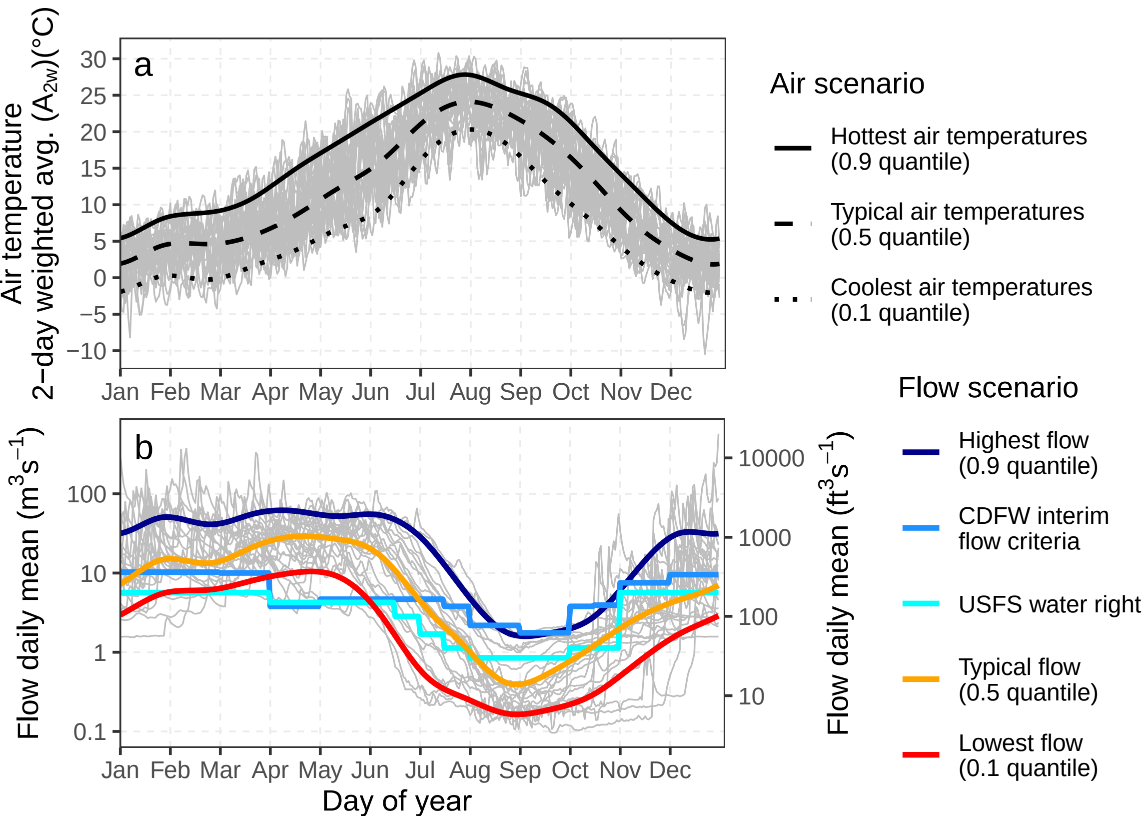

a
Air temperature
2−day weighted avg. (A_{2w})(°C)
30
25
20
15
10
5
0
−5
−10
Jan Feb Mar Apr May Jun Jul Aug Sep Oct Nov Dec
Air scenario
Hottest air temperatures (0.9 quantile)
Typical air temperatures (0.5 quantile)
Coolest air temperatures (0.1 quantile)
b
Flow daily mean (m^3s^{-1})
100
10
1
0.1
Flow daily mean (ft^3s^{-1})
10000
1000
100
10
Jan Feb Mar Apr May Jun Jul Aug Sep Oct Nov Dec
Day of year
Flow scenario
Highest flow (0.9 quantile)
CDFW interim flow criteria
USFS water right
Typical flow (0.5 quantile)
Lowest flow (0.1 quantile)

Figure 4.

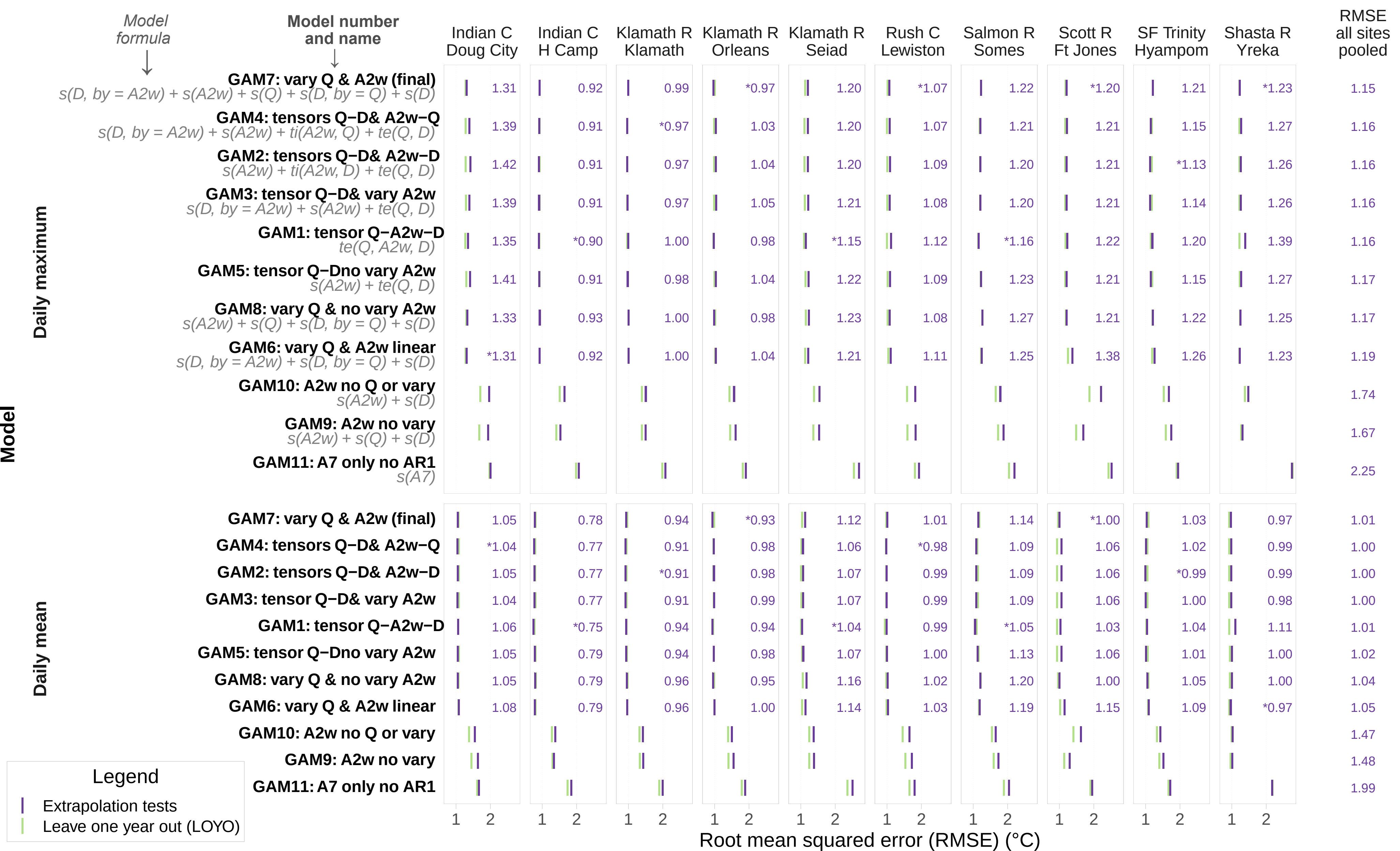

Model formula
Model number and name
Indian C Doug City
Indian C H Camp
Klamath R Klamath
Klamath R Orleans
Klamath R Seiad
Rush C Lewiston
Salmon R Somes
Scott R Ft Jones
SF Trinity Hyampom
Shasta R Yreka
RMSE all sites pooled
Model
Daily maximum
GAM7: vary Q & A2w (final)
s(D, by = A2w) + s(A2w) + s(Q) + s(D, by = Q) + s(D)
1.31 0.92 0.99 *0.97 1.20 *1.07 1.22 *1.20 1.21 *1.23 1.15
GAM4: tensors Q−D& A2w−Q
s(D, by = A2w) + s(A2w) + ti(A2w, Q) + te(Q, D)
1.39 0.91 *0.97 1.03 1.20 1.07 1.21 1.21 1.15 1.27 1.16
GAM2: tensors Q−D& A2w−D
s(A2w) + ti(A2w, D) + te(Q, D)
1.42 0.91 0.97 1.04 1.20 1.09 1.20 1.21 *1.13 1.26 1.16
GAM3: tensor Q−D& vary A2w
s(D, by = A2w) + s(A2w) + te(Q, D)
1.39 0.91 0.97 1.05 1.21 1.08 1.20 1.21 1.14 1.26 1.16
GAM1: tensor Q−A2w−D
te(Q, A2w, D)
1.35 *0.90 1.00 0.98 *1.15 1.12 *1.16 1.22 1.20 1.39 1.16
GAM5: tensor Q−Dno vary A2w
s(A2w) + te(Q, D)
1.41 0.91 0.98 1.04 1.22 1.09 1.23 1.21 1.15 1.27 1.17
GAM8: vary Q & no vary A2w
s(A2w) + s(Q) + s(D, by = Q) + s(D)
1.33 0.93 1.00 0.98 1.23 1.08 1.27 1.21 1.22 1.25 1.17
GAM6: vary Q & A2w linear
s(D, by = A2w) + s(D, by = Q) + s(D)
*1.31 0.92 1.00 1.04 1.21 1.11 1.25 1.38 1.26 1.23 1.19
GAM10: A2w no Q or vary
s(A2w) + s(D)
1.74
GAM9: A2w no vary
s(A2w) + s(Q) + s(D)
1.67
GAM11: A7 only no AR1
s(A7)
2.25
Daily mean
GAM7: vary Q & A2w (final)
1.05 0.78 0.94 *0.93 1.12 1.01 1.14 *1.00 1.03 0.97 1.01
GAM4: tensors Q−D& A2w−Q
*1.04 0.77 0.91 0.98 1.06 *0.98 1.09 1.06 1.02 0.99 1.00
GAM2: tensors Q−D& A2w−D
1.05 0.77 *0.91 0.98 1.07 0.99 1.09 1.06 *0.99 0.99 1.00
GAM3: tensor Q−D& vary A2w
1.04 0.77 0.91 0.99 1.07 0.99 1.09 1.06 1.00 0.98 1.00
GAM1: tensor Q−A2w−D
1.06 *0.75 0.94 0.94 *1.04 0.99 *1.05 1.03 1.04 1.11 1.01
GAM5: tensor Q−Dno vary A2w
1.05 0.79 0.94 0.98 1.07 1.00 1.13 1.06 1.01 1.00 1.02
GAM8: vary Q & no vary A2w
1.05 0.79 0.96 0.95 1.16 1.02 1.20 1.00 1.05 1.00 1.04
GAM6: vary Q & A2w linear
1.08 0.79 0.96 1.00 1.14 1.03 1.19 1.15 1.09 *0.97 1.05
GAM10: A2w no Q or vary
1.47
GAM9: A2w no vary
1.48
GAM11: A7 only no AR1
1.99
1 2
Root mean squared error (RMSE) (°C)
Legend
Extrapolation tests
Leave one year out (LOYO)

Figure 5.

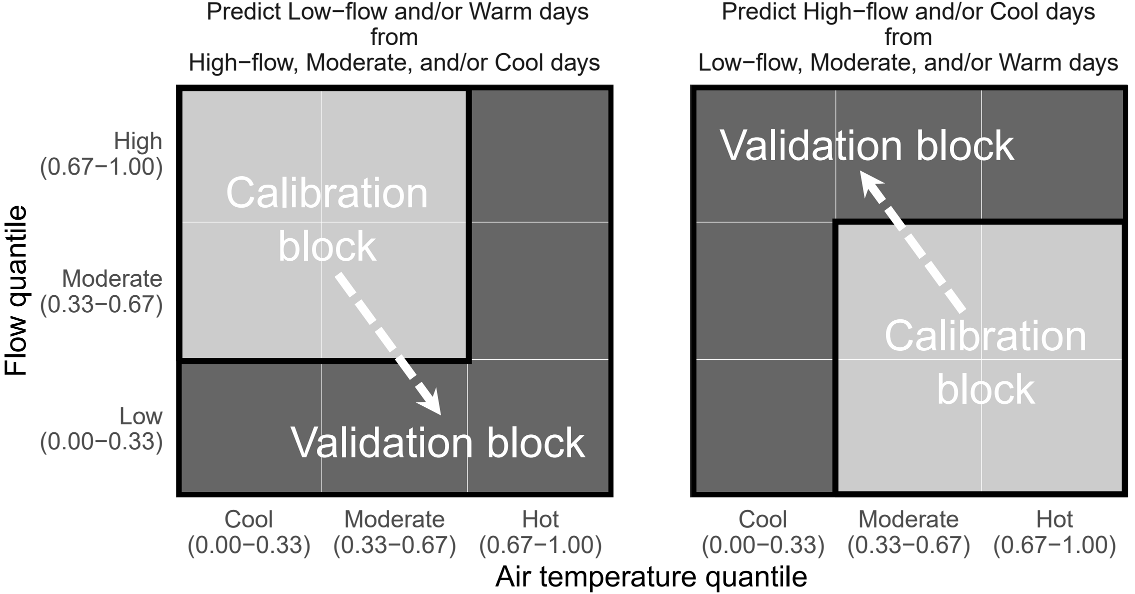
Predict Low−flow and/or Warm days
from
High−flow, Moderate, and/or Cool days
Predict High−flow and/or Cool days
from
Low−flow, Moderate, and/or Warm days
Calibration block
Validation block
Validation block
Calibration block
Flow quantile
High (0.67−1.00)
Moderate (0.33−0.67)
Low (0.00−0.33)
Cool (0.00−0.33)
Moderate (0.33−0.67)
Hot (0.67−1.00)
Cool (0.00−0.33)
Moderate (0.33−0.67)
Hot (0.67−1.00)
Air temperature quantile

Figure 6.

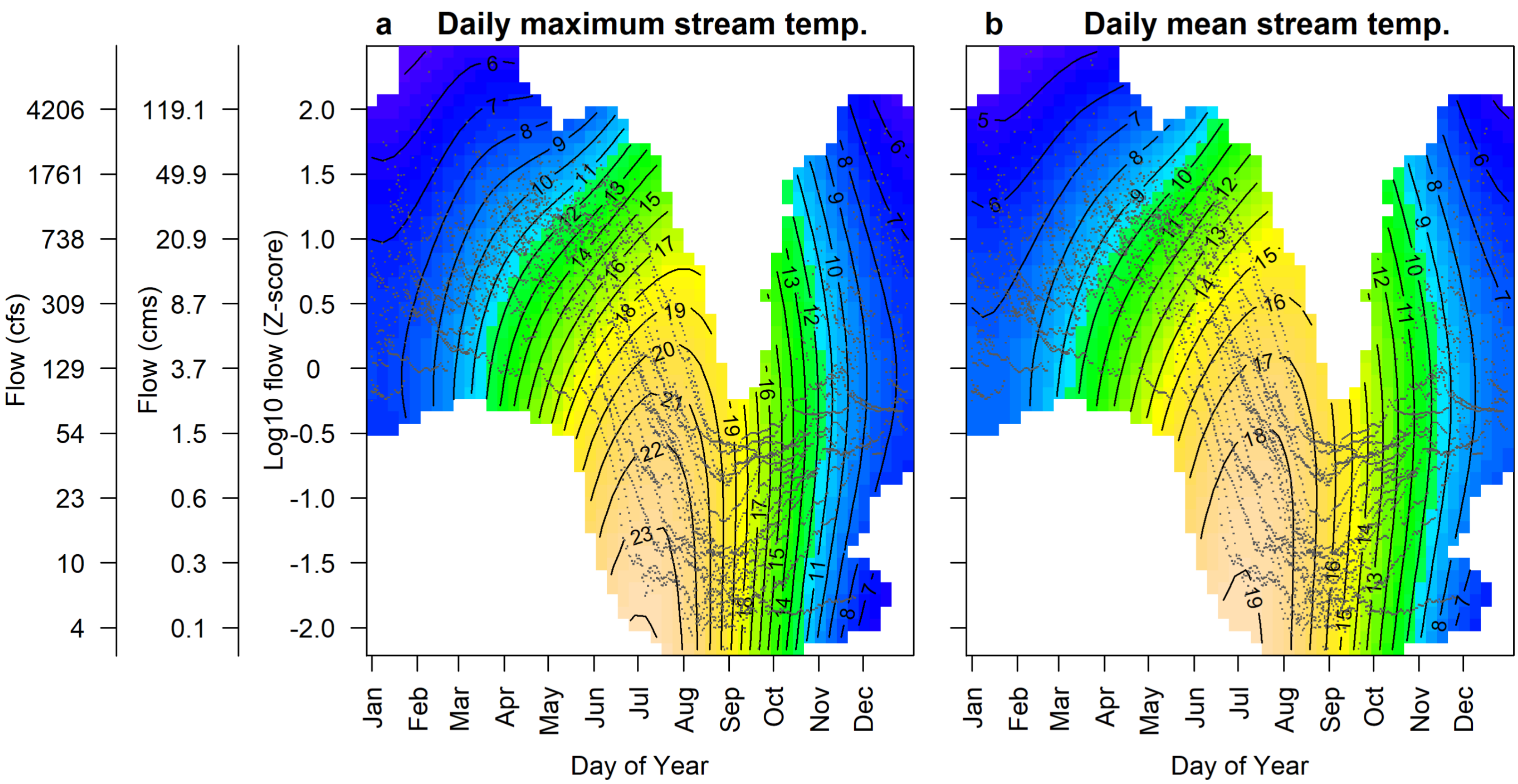

a Daily maximum stream temp.
b Daily mean stream temp.
Flow (cfs)
Flow (cms)
Log10 flow (Z-score)
4206
1761
738
309
129
54
23
10
4
119.1
49.9
20.9
8.7
3.7
1.5
0.6
0.3
0.1
2.0
1.5
1.0
0.5
0
-0.5
-1.0
-1.5
-2.0
Jan
Feb
Mar
Apr
May
Jun
Jul
Aug
Sep
Oct
Nov
Dec
Day of Year

Figure 7.

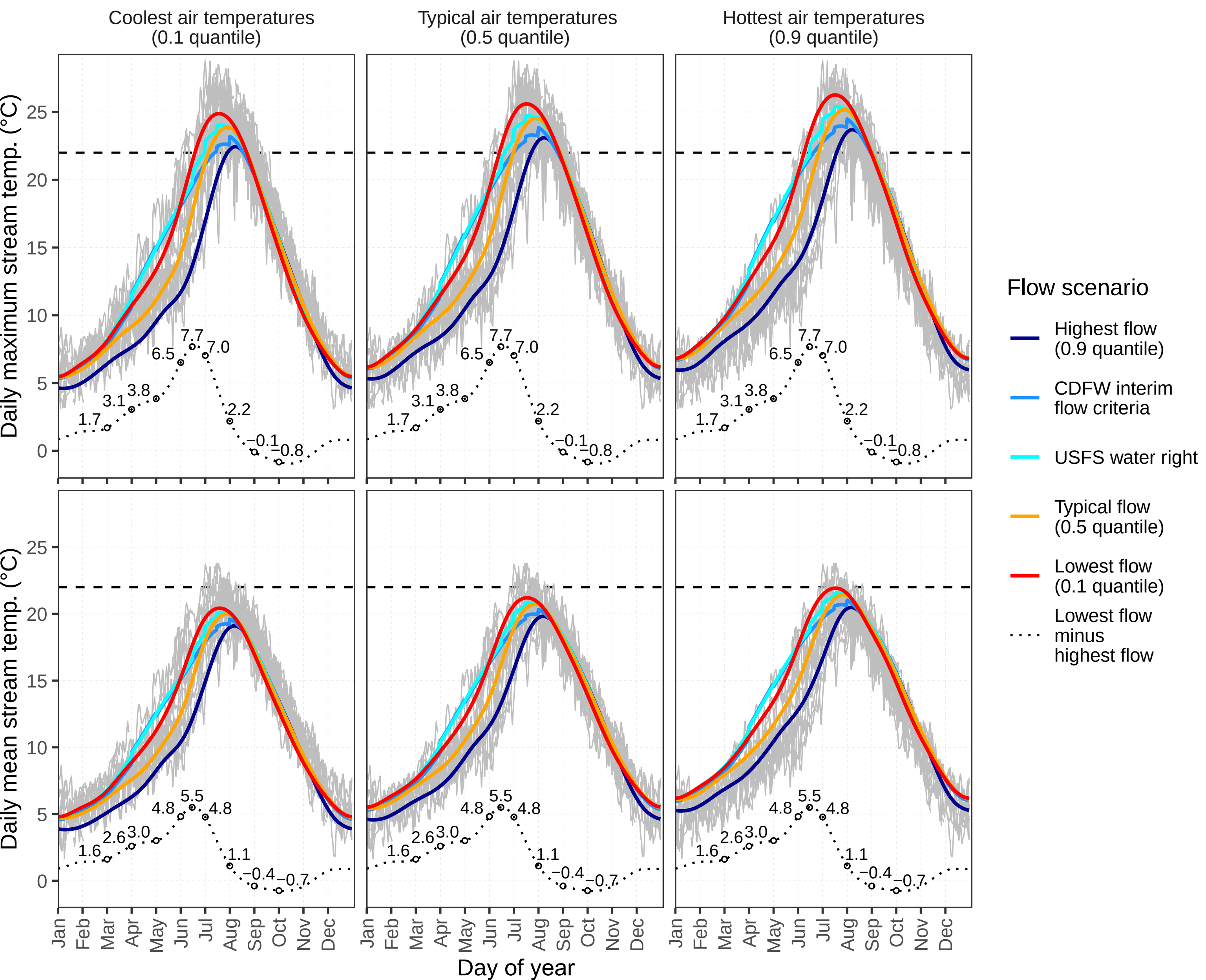

Coolest air temperatures
(0.1 quantile)
Typical air temperatures
(0.5 quantile)
Hottest air temperatures
(0.9 quantile)
Daily maximum stream temp. (°C)
Daily mean stream temp. (°C)
Day of year
Jan
Feb
Mar
Apr
May
Jun
Jul
Aug
Sep
Oct
Nov
Dec
0
5
10
15
20
25
1.7
3.1
3.8
6.5
7.7
7.0
2.2
−0.1
−0.8
1.6
2.6
3.0
4.8
5.5
4.8
1.1
−0.4
−0.7
Flow scenario
Highest flow
(0.9 quantile)
CDFW interim
flow criteria
USFS water right
Typical flow
(0.5 quantile)
Lowest flow
(0.1 quantile)
Lowest flow
minus
highest flow

Figure 8.

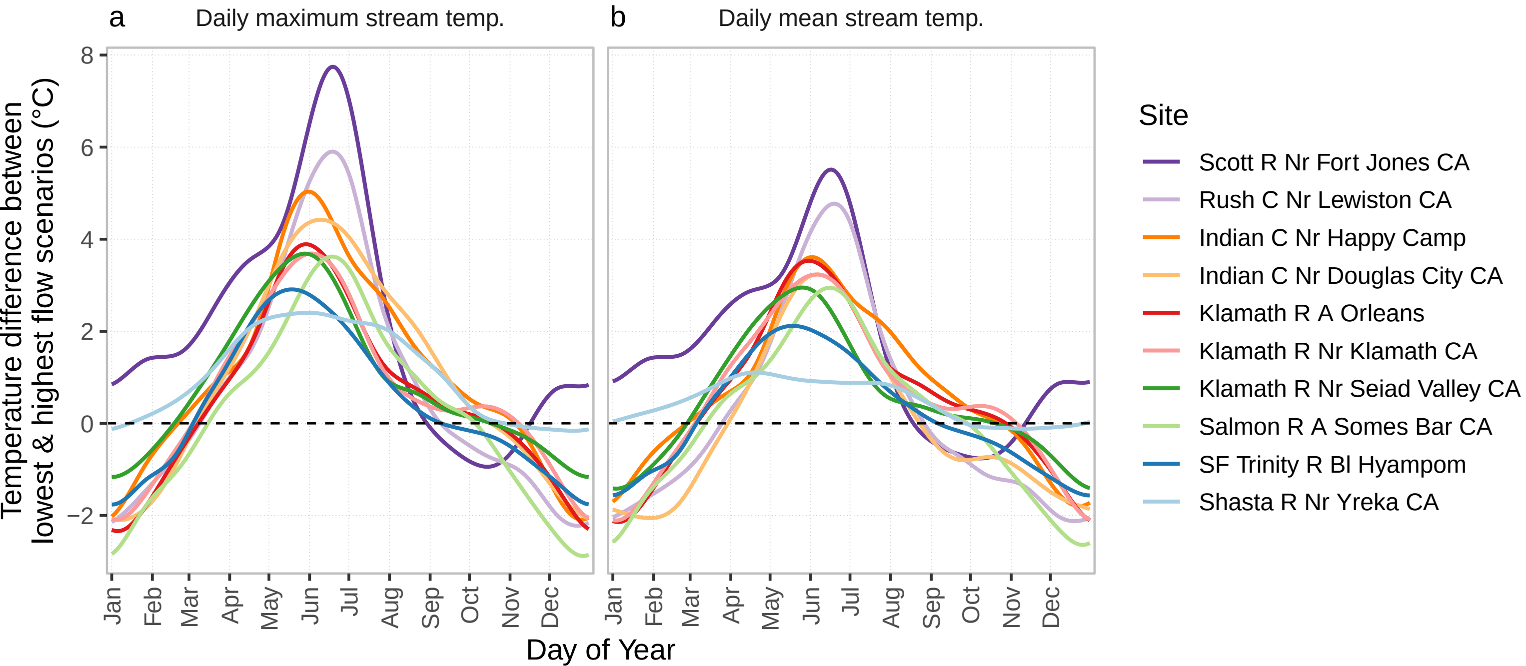

a
Daily maximum stream temp.
b
Daily mean stream temp.
Temperature difference between lowest & highest flow scenarios (°C)
8
6
4
2
0
−2
Jan
Feb
Mar
Apr
May
Jun
Jul
Aug
Sep
Oct
Nov
Dec
Day of Year
Site
Scott R Nr Fort Jones CA
Rush C Nr Lewiston CA
Indian C Nr Happy Camp
Indian C Nr Douglas City CA
Klamath R A Orleans
Klamath R Nr Klamath CA
Klamath R Nr Seiad Valley CA
Salmon R A Somes Bar CA
SF Trinity R Bl Hyampom
Shasta R Nr Yreka CA

Figure 9.

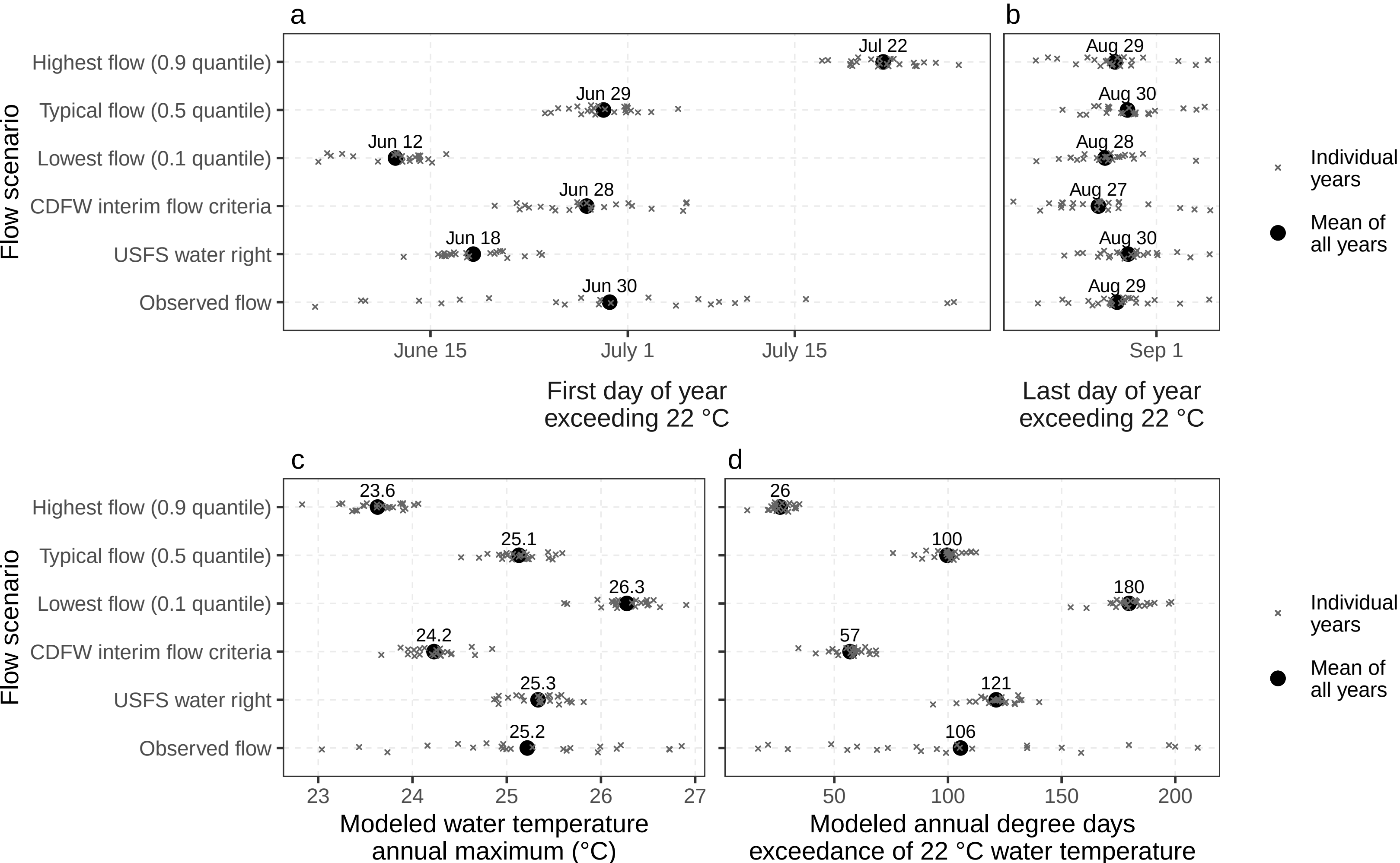
a
b
Highest flow (0.9 quantile)
Typical flow (0.5 quantile)
Lowest flow (0.1 quantile)
CDFW interim flow criteria
USFS water right
Observed flow
Flow scenario
Jul 22
Jun 29
Jun 12
Jun 28
Jun 18
Jun 30
June 15
July 1
July 15
First day of year exceeding 22 °C
Aug 29
Aug 30
Aug 28
Aug 27
Aug 30
Aug 29
Sep 1
Last day of year exceeding 22 °C
Individual years
Mean of all years
c
d
23.6
25.1
26.3
24.2
25.3
25.2
23
24
25
26
27
Modeled water temperature annual maximum (°C)
26
100
180
57
121
106
50
100
150
200
Modeled annual degree days exceedance of 22 °C water temperature

Water Resources Research

Supporting Information for

Modeling Seasonal Effects of River Flow on Water Temperatures in an Agriculturally Dominated California River

J. Eli Asarian[1], Crystal Robinson[2†], Laurel Genzoli[3]

[1]Riverbend Sciences, Eureka, CA, USA, [2]Quartz Valley Indian Reservation, Fort Jones, CA, USA, [3]Flathead Lake Biological Station and the University of Montana in Missoula, MT, USA, [†]current affiliation: California Department of Fish and Wildlife, Yreka, CA, USA

Contents of this file

Text S1 to S6
Tables S1 to S2
Figures S1 to S15

Introduction

The supporting text contains methodological details on quality control procedures and combining of stream temperature data from multiple entities (Text S1), choosing autocorrelation coefficients in the GAMs and why we included a random effect for year (Text S3, Figures S12, S13, S14), and additional discussion of the 22 °C salmonid temperature threshold (Text S4) that were excluded from the manuscript for the sake of brevity. A sensitivity analysis on the effects of using different methods for summarizing air temperatures is provided in Text S2 and Figure S11. Text S6 discusses the modal relationship between flow and stream temperature at some sites during the October–November period. Supporting figures include additional outputs from the stream temperature models, including time series plots comparing modeled data to observed data (Figures S5, S6, and S7), a GAM smoother plot (Figure S3), Bayesian information criteria scores (Figure S4 and accompanying Text S5), daily outputs from model scenarios (Figure S8); and standardized flow coefficients from previous regional studies (Figure S9, S10). Table S1 provides site characteristics and data sources for stream temperature modeling sites. Table S2 lists mean ranks for each model.

Text S1.

Primary quality control was conducted by the entities who collected the stream temperature data. These entities check probe calibration before and after every deployment, and data not meeting calibration criteria are discarded. In addition, we reviewed the data and removed any suspicious values (e.g., when there were calibration issues or probes appear to have been exposed to air). The Quartz Valley Indian Reservation (QVIR) Environmental Department uses YSI (Yellow Springs, Ohio) 6600 multi-parameter datasondes to monitor Scott River water temperatures at the U.S. Geological Survey (USGS) gage 11519500 near the outlet of Scott Valley (QVIR, 2016; Asarian et al., 2020), recording temperature measurements every 30 minutes with a reported accuracy of ±0.15 °C. The YSI 6600 multi-parameter datasondes do not require calibration but are compared to a reference sonde every two weeks and serviced by the manufacturer annually (QVIR, 2016). KNF's stream temperature monitoring equipment has changed over time, but calibration and deployment protocol has remained similar with pre- and post-deployment testing against a National Institute of Standards and Technology (NIST) traceable thermometer (KNF, 2010, 2011). Since 2010, KNF has used ONSET Pro v2 data logger u22-001 for all temperature monitoring (KNF, 2011). Prior to 2010 KNF used a combination of ONSET Pro v2 u22-001, Optic StowAway, and other ONSET temperature logger models. USFWS protocols are described by Romberger & Gwozdz (2018). USBR data were subjected to a detailed quality control review by USGS prior to inclusion in the database from which we accessed them (Smith et al., 2018).

For days on which Scott River daily stream temperatures were available from multiple entities, we averaged the values together. For the 1216 days with both QVIR and USFS records, root mean standard error (RMSE) was 0.31 °C and 0.18 °C for T_{max} and T_{mean}, and respectively. Only one entity collected data at each of the other nine sites, so averaging values was unnecessary there.

Text S2.

At the beginning of this project, we only modeled stream temperatures at the Scott River site. Our final analyses at all 10 Klamath Basin sites use a 2-day weighted average air temperatures (A_{2w}) from the gridded PRISM air temperature dataset (Daly et al., 2008); however, for the initial Scott River analyses, we used daily mean air temperature data from USFS' Quartz Hill weather station (Global Historical Climatology Network - Daily [GHCND] station USR0000CQUA; Menne et al., 2012a, 2012b) located approximately 8 km southeast of the stream temperature gage, with missing values infilled by linear regression with nearby weather stations or PRISM. In initial explorations of Scott River stream temperature models, we explored many air temperature metrics including multi-day averages (Webb et al., 2003; Siegel et al. 2022), exponential weights (Koch & Grünewald, 2010; Piotrowski & Napiorkowski, 2019; Soto, 2016), and including the day of interest and preceding days separately (Siegel & Volk 2019). These explorations tested five categories of air temperature metrics, where A_i is the mean air temperature on the day *i*, using Equations (1), (2), (3), (4), and (5):

Single-day average A_1:

$$A_1 = A_i \tag{1}$$

Multi-day averages $A_2 \ldots A_7$:

$$A_2 = \frac{(A_i + A_{i-1})}{2}, \ldots, A_7 = \frac{(A_i + A_{i-2} \ldots A_{i-6})}{7} \tag{2}$$

Multi-day weighted averages A_{2w} and A_{3w}, with preceding days discounted by 50% per day:

$$A_{2w} = \frac{A_i + (0.5 \times A_{i-1})}{1.5} \quad \text{and} \quad A_{3w} = \frac{(A_i + 0.5A_{i-1} + 0.25A_{i-2})}{1.75} \tag{3}$$

Lagged averages A_{L3} and A_{L5}:

$$A_{L3} = \frac{(A_{i-1} + A_{i-2} + A_{i-3})}{3} \quad \text{and} \quad A_{L5} = \frac{(A_{i-1} + A_{i-2} + A_{i-3} + A_{i-4} + A_{i-5})}{5} \tag{4}$$

Differences between lagged average and day *i*:

$$A_{\Delta 3} = (A_i - A_{L3}) \quad \text{and} \quad A_{\Delta 5} = (A_i - A_{L5}) \tag{5}$$

These initial Scott River explorations, using a model structure similar to GAM4 (tensors for Q-D and A2w-D), indicated that the 2-day weighted air temperature (A_{2w}) had excellent performance for predicting both T_{max} and T_{mean}, so we proceeded to use A_{2w} for all subsequent stream temperature models except one that uses a seven-day average (A_7) (Section 3.2).

After completing our final modeling at all 10 sites using PRISM A_{2w} (or A_7) and selecting our final model GAM7, we did a sensitivity analysis comparing performance of variants of Scott River GAM7 using the same air temperature summaries that were initially tested, except this time using data from PRISM instead of the local GHCND weather station measurements. Interestingly, the results of this GAM7 PRISM sensitivity analysis (Figure S11) differed from the initial GAM4 GHCND sensitivity analysis (not shown here), with the single-day average A_1 performing better (i.e., lower RMSE and BIC) than A_{2w}. Surprised, we explored further (i.e., ran a similar sensitivity analysis on GAM4 PRISM, results not shown here) and determined that which air temperature summary worked the best (i.e., A_1 or A_{2w}) was not due to differences between the modeling structure of GAM4 and GAM7 (i.e., tensors or non-linear smoothers, etc.) but rather between the PRISM data and

GHCND data. We speculate, but did not confirm, that this may be due to differences in how days are defined between PRISM and GHCND. In summarizing daily stream temperatures, we defined days as midnight-to-midnight local time, but PRISM days are defined at 1200–1200 UTC (e.g., 0700–0700 EST) and stations with reporting times (i.e., day definition) within four hours are used as inputs to PRISM (Daly et al. 2021). We could not readily ascertain the reporting time for the GHCND station we used.

Text S3.

The bam in mgcv function cannot automatically derive the AR-1 coefficient (rho), so it must be manually assigned. Following Baayen et al. (2018) and van Rij et al. (2019, 2020), we initially fit each model without an autocorrelation term, and then re-ran the model with an autocorrelation term, assigning a rho value based on the lag 1 autocorrelation from the residuals of the initial model. Comparing models fit using fast restricted maximum likelihood (fREML) with a range of rho values, as recommended by Baayen et al. (2018), van Rij et al. (2019), and Wood (2017), confirmed these initial values were reasonable. These tests indicated that rho values that minimized fREML scores were 0.02–0.16 higher than the initial rho values (Figure S12 shows example of Scott River GAM7, Figure S13 shows all models for all sites). However, autocorrelation function (ACF) plots indicated that these higher rho values often had the undesirable side effect of exacerbating the negative autocorrelation at lag 1 or lag 2 (e.g., Figure S14 shows example of Scott River GAM7), leading to our decision to use the initial rho values instead. BIC scores, included as a supplementary measure of model fit, show the same pattern as fREML scores regarding optimal rho values (Figure S12). Using BIC scores to assess optimal rho values in fREML-fit models is acceptable because the models compared had the same fixed effects and differed only in their rho values.

A random effect for year was included to account for year-to-year variability in other factors not included in the models such as changes in channel morphology or riparian vegetation. From a statistical perspective, including a random effect for year is beneficial because it helps reduce temporal autocorrelation within years that arises from a combination of the natural hierarchical structure of both the physical system (i.e., see previous sentence) and how the data were collected. For example, some sites and years have data for summer only (or other periods that do not span across multiple years), so for those years the random effect would account for differences in the exact placement of the temperature probe and/or any bias in the probe itself. However, we acknowledge for those sites and years when data were collected year-round and the probes were visited multiple times per year, year would be less of a natural break.

Text S4.

We chose 22 °C as an indicator of biological effects on juvenile salmonids that rear in the mainstem Scott River or outmigrate downstream using the river as a migratory corridor.

Given the potential for local genetic adaptation to thermal regimes (Zillig et al., 2021), we prioritized geographically proximal studies in selecting thresholds. When the Klamath River exceeds 22–23 °C, juvenile salmonids move to tributary confluences (Brewitt & Danner, 2014; Sutton & Soto, 2012; Sutton et al., 2007). Similar behavior was observed in the Shasta River (Nichols et al., 2014) and 22 °C was also used by McGrath et al. (2017). In recognition of our study site's location on a mainstem river where temperatures would naturally be higher than a small well-shaded or spring-fed tributary, we chose 22 °C over colder thresholds that would more fully protect coho salmon like Stenhouse et al.'s (2012) recommendation of 15.5 °C for spring-fed tributaries to the Shasta River or Welsh et al.'s (2001) 18 °C maximum weekly maximum temperature (MWMT) derived from coastal streams. In addition, juvenile coho salmon grew fast in experimental cages in the food-rich Shasta River with MWMT as high as 24.0 °C, although survival was higher at cooler sites (Lusardi et al., 2019). Our data and code are public, so future researchers could choose a different threshold. Recognizing the drawbacks of any single statistic or threshold (Steel et al., 2013), we also examine annual maximum temperature.

Text S5.

BIC scores (Figure S4) largely corroborate the extrapolation CV results identifying the importance of seasonally varying flow effects. Of eight models with seasonally varying flow effects, the most complex model (three-way tensor GAM1) had the worst overall (averaged across all sites) BIC rank, but intermediate extrapolation CV RMSE. Averaging BIC ranks across sites, our extrapolation CV-selected model, GAM7, had the best BIC ranks for both Tmax and Tmean (Figure S4); however, at many individual sites including Scott River, other models had better BIC scores (Figure S4).

Text S6.

At Scott River (Figure 6) and two other sites (Figure S15), the modeled flow-temperature relationship is modal (i.e., highest water temperatures at moderate flows) instead of monotonic in October–November, a period of hydrologic transition when precipitation ends seasonal baseflow recession, increases flow, and refills the valley aquifer (Figure 1). The reasons for this non-monotonic behavior are unclear, but could reflect processes such as groundwater-surface water dynamics, variation in timing of fall precipitation, or other seasonal variables; regardless, these departures from monotonic are of low consequence because they are <1 °C and occur when temperatures are not a biological concern.

Table S1. Site characteristics and data sources for stream temperature modeling sites. Drainage areas are from NHDPlus version 2.1 (Moore & Dewald, 2016). Key to abbreviations: CDWR = California Department of Water Resources, QVIR = Quartz Valley Indian Reservation, USBR = U.S. Bureau of Reclamation, USFWS = U.S. Fish and Wildlife Service, USFS KNF = United States Forest Service Klamath National Forest, and USGS = U.S. Geological Survey.

		Stream temperature data							
Site number and name of USGS flow gage	Drainage area (km^2)	Data source	Original site code	N. of days	N. of years	Date range	Latitude	Longitude	Notes
11530500 Klamath R Nr Klamath CA	34550	USFWS	KRTG2	5002	16	2004–2019	41.51118	-123.97844	
11523000 Klamath R A Orleans	25159	USFWS	KROR1	4138	17	2001–2018	41.30358	-123.53439	
11520500 Klamath R Nr Seiad Valley CA	21171	USFWS	KRSV1	5684	19	2001–2019	41.85409	-123.23147	
11528700 SF Trinity R Bl Hyampom	2414	USFWS	SFTR1	4627	19	2001–2019	40.88943	-123.60221	Temperature monitoring site located at confluence with Trinity River, 42.5 km downstream of the USGS gage
11522500 Salmon R A Somes Bar CA	1946	CDWR	F3410000	5200	18	2002–2019	41.37695	-123.47736	
11517500 Shasta R Nr Yreka CA	1934	USFWS	SHKR1	5172	18	2001–2019	41.82476	-122.59392	
11519500 Scott R Nr Fort Jones CA	1716	QVIR	SRGA	3180	13	2007–2020	41.64000	-123.01380	
		USFS KNF	H2O_Temp_LOCID103	977	8	2006–2016			
		USFS KNF	H2O_Temp_ScottNearFtJones	1048	3	2009–2011			
		USBR	11519500	682	3	1998–2000			
		USFS KNF	Scott River at USGS Gage	341	3	2003–2019			
		USFS KNF	H2O_Temp_LOCID224	118	1	2004–2004			
11521500 Indian C Nr Happy Camp	310	USFS KNF	H2O_Temp_LOCID056	3540	17	2000–2016	41.83525	-123.38291	
11525670 Indian C Nr Douglas City CA	87	USFWS	ICTR1	5197	18	2002–2019	40.65645	-122.91388	
11525530 Rush C Nr Lewiston CA	58	USBR/USGS	RCL	5679	18	2001–2019	40.72500	-122.83400	

Table S2. Overall model ranks from extrapolation cross-validation tests, each calculated as mean RMSE rank of all 10 sites and both temperature response variables (T_{max} and T_{mean}). See Figure 4 for model formulas and a key to abbreviations.

Model number and name	Mean rank RMSE
GAM7: vary Q & A2w (final)	3.60
GAM2: tensors Q-D & A2w-D	3.65
GAM4: tensors Q-D & A2w-Q	3.65
GAM3: tensor Q-D & vary A2w	3.80
GAM1: tensor Q-A2w-D	4.10
GAM5: tensor Q-D no vary A2w	5.10
GAM8: vary Q & no vary A2w	5.70
GAM6: vary Q & A2w linear	6.55
GAM10: A2w no Q or vary	9.40
GAM9: A2w no vary	9.45
GAM11: A7 only no AR1	11.00

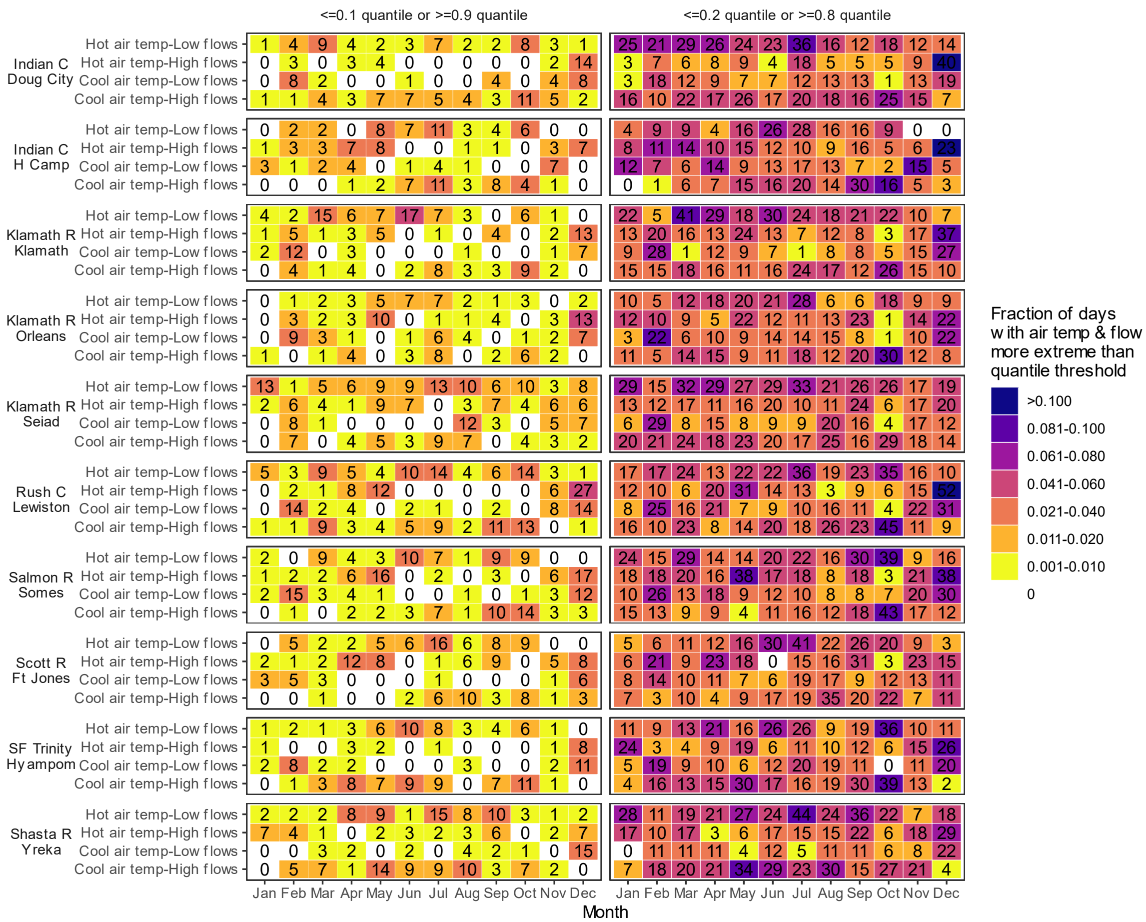

Figure S1. Availability of measured water temperature data for days when extreme quantiles of air temperature and flow co-occur. Shading indicates the fraction of days for each site and month when air temperatures and flow were more extreme than the quantile threshold (≤0.1 and ≥0.9 for left panels, ≤0.2 and ≥0.8 for right panels). Data labels inside each square indicate the total number of days exceeding the quantile threshold. For example, in July at Scott River there were 16 days (2.8% of the 572 days when water temperature data were available for that site and month) when air temperatures were ≥0.9 quantile and flows were ≤0.1 quantile.

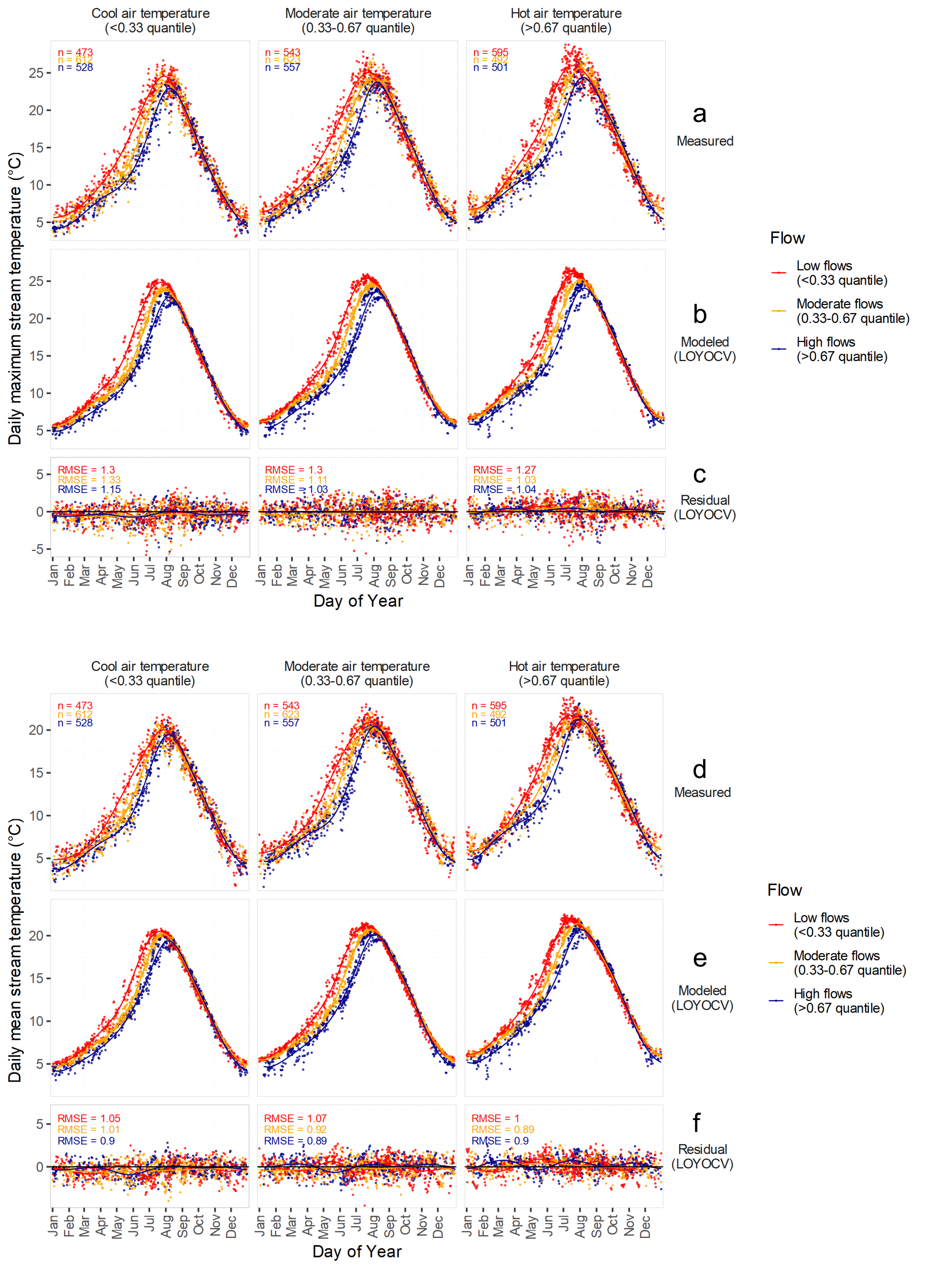

Figure S2. Measured (a) T_{max} and (d) T_{mean} at Scott River for dates with combinations of cool, typical, or hot air temperatures (arranged in columns) and low, typical, or high flows (shown by color). (b,e) Modeled LOYO CV temperatures predicted by selected model GAM7 for the same dates, and (c,f) LOYO CV residuals, calculated as measured minus modeled. Lines are GAM smoothers fit to points, shown as visual aids.

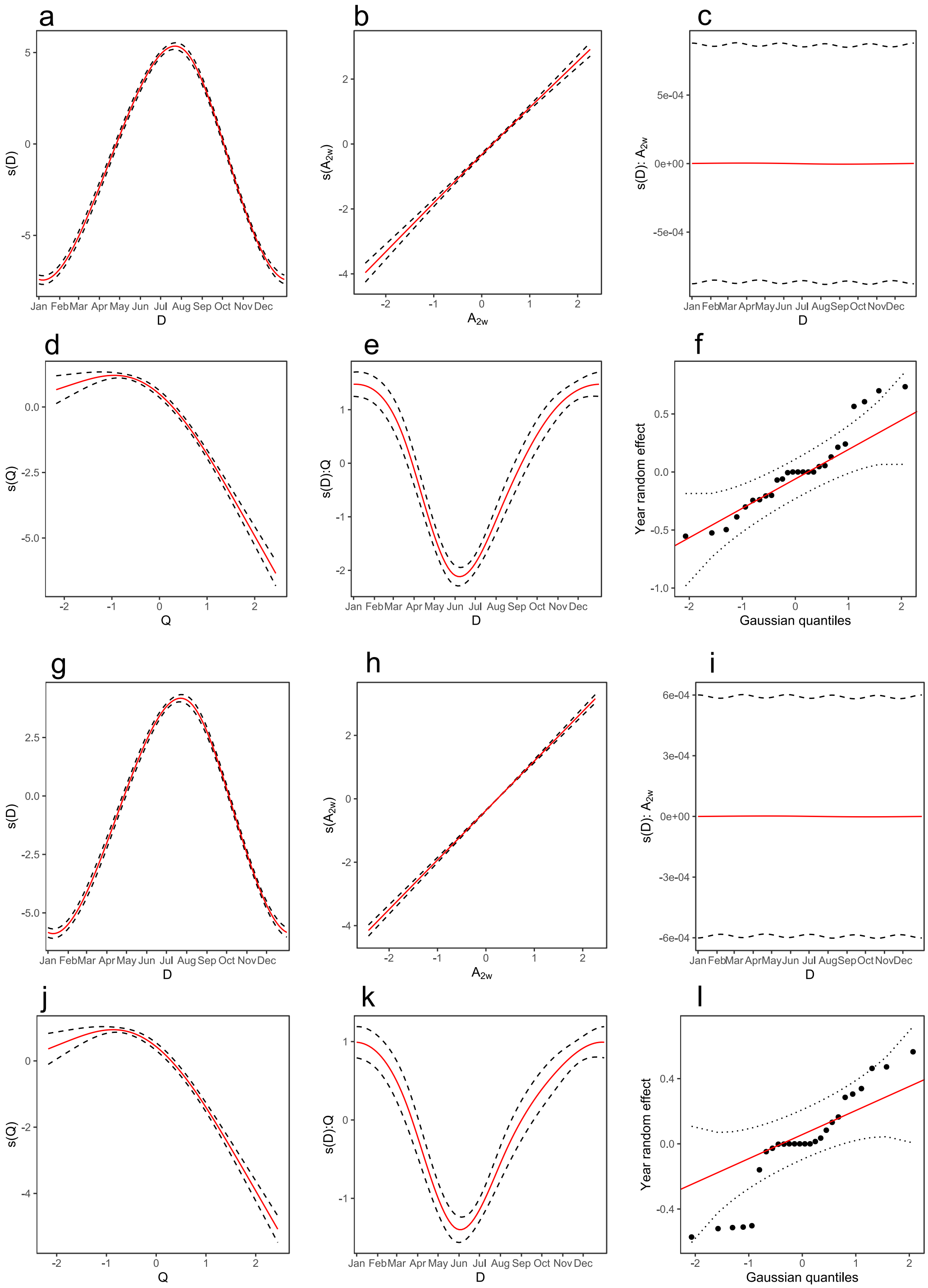

Figure S3. GAM smooths (i.e., covariate responses and interactions) from Scott River model GAM7 for T_{max} (top six panels) and T_{mean} (bottom six panels) showing partial effects of smooth functions of: (a,g) day of year D, (b,h) two-day air temperature A2w, (c,i) interaction of A_{2w} and D (i.e, slope of A_{2w} varying as non-linear function of D), (d,j) flow Q, and (e,k) interaction of Q and D. Dashed lines are 95% confidence intervals. (f,l) shows random effects for year.

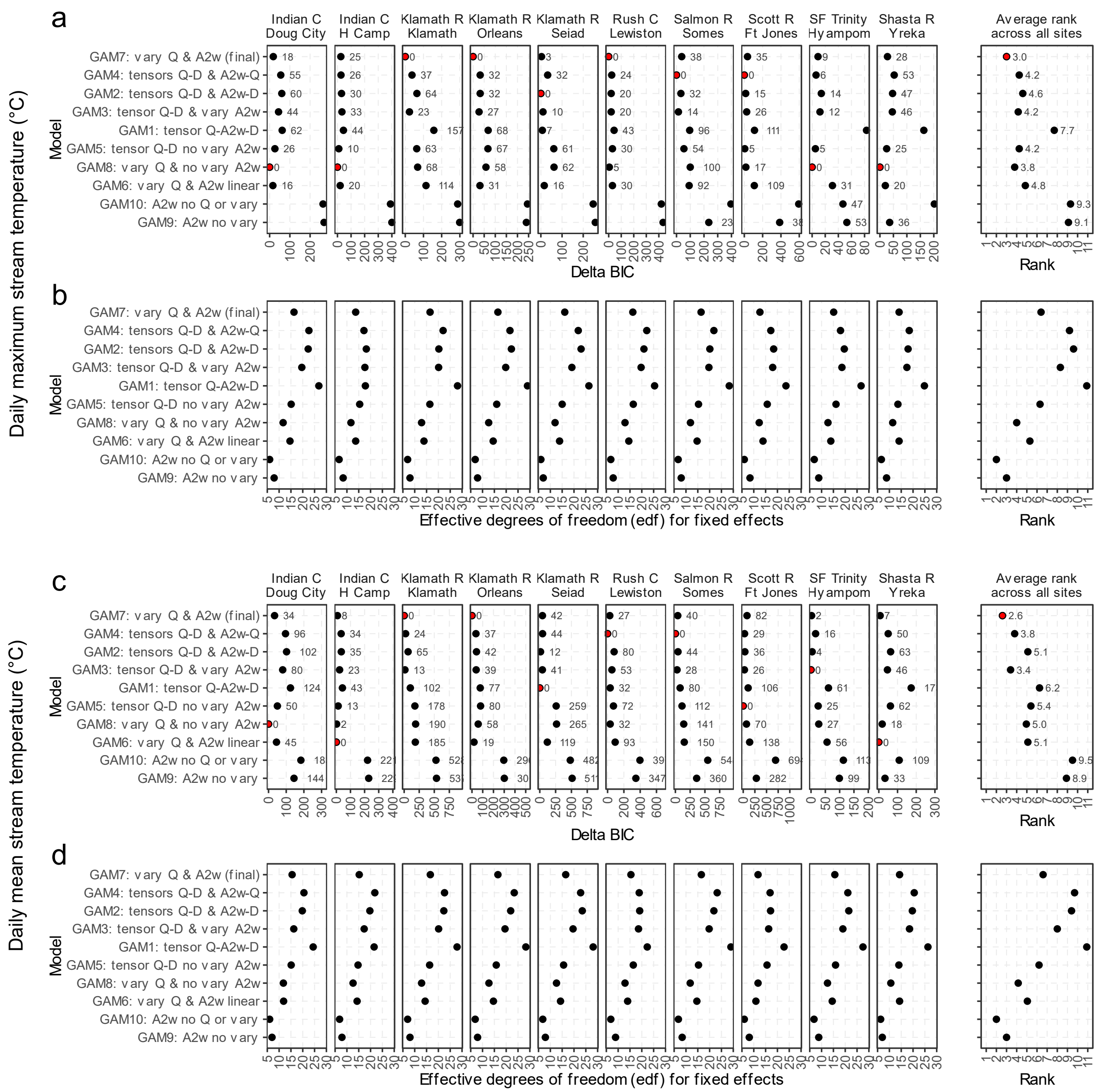

Figure S4. Comparison of (a,c) delta BIC, and (b,d) effective degrees of freedom (edf) for models of (a,b) T_{max} and (c,d) T_{mean} at 10 sites in the Klamath Basin. Symbols for models with lowest delta BIC are colored red. Models are sorted in same order as in Figure 4 (i.e., by overall RMSE rank). Average ranks in right column were calculated by first ranking model scores within each site (i.e., 1=best, 11=worst), then averaging those model ranks across sites. Model GAM11 was excluded from this figure because its model fit was so poor it would expand the axes making it difficult to see differences between the other models.

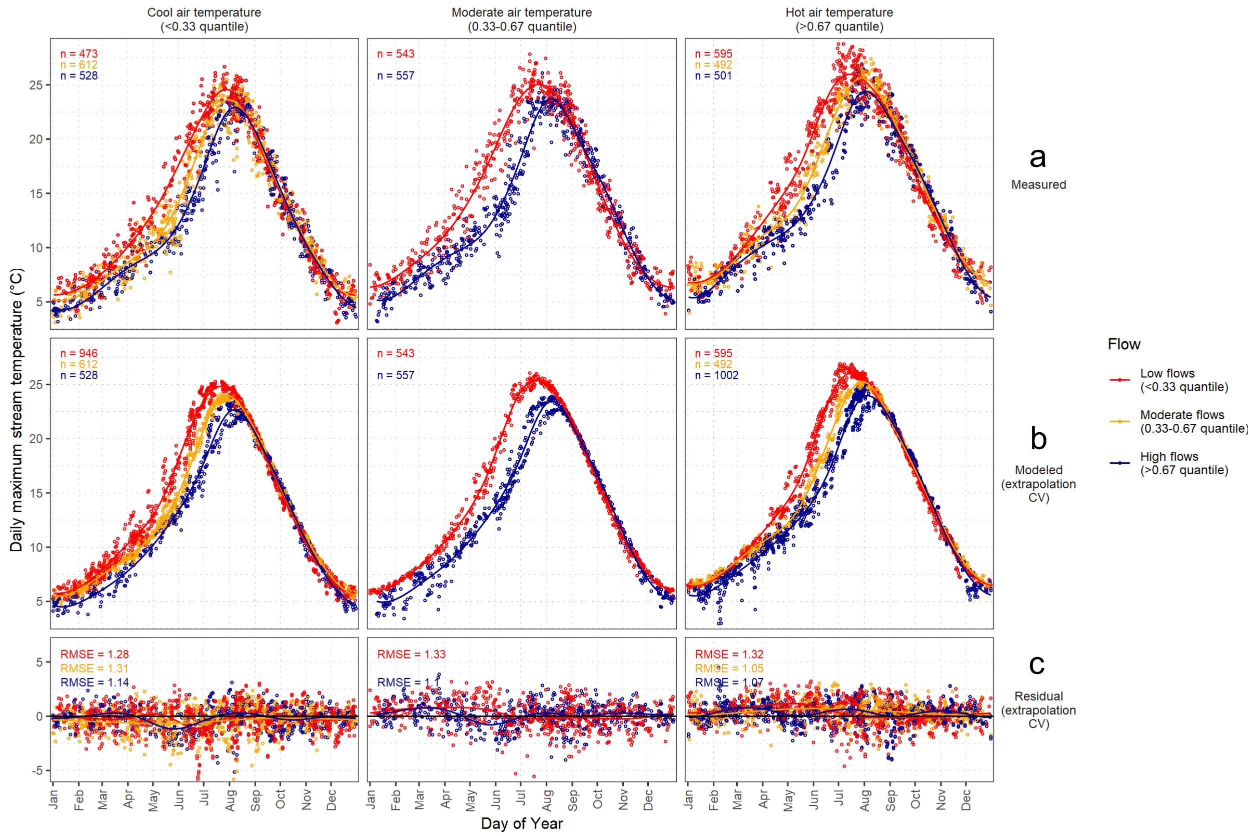

Figure S5. (a) Measured T_{max} at Scott River for dates with combinations of cool, moderate, or hot air temperatures (arranged in columns) and low, moderate, or high flows (shown by color). (b) Modeled extrapolation CV temperatures predicted by the selected model 'GAM7' for the same dates, and (c) extrapolation CV residuals, calculated as measured minus modeled. Lines are GAM smoothers fit to the points, shown as visual aids.

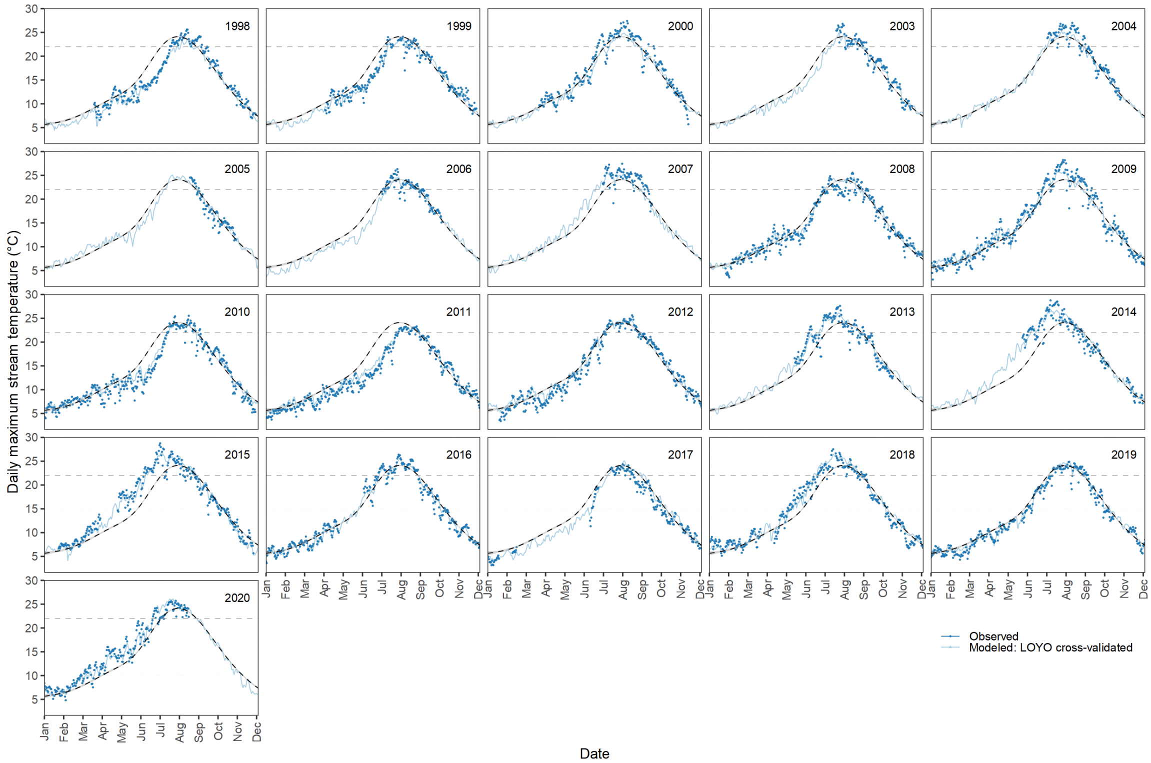

Figure S6. Daily time series of measured (dots) and modeled (solid lines, from leave-one-year-out [LOYO] cross-validation) T_{max} in the Scott River at the USGS gage for the years 1998–2020 (no data 2001-2002). Horizontal dashed gray line at 22 °C indicates a temperature threshold for juvenile salmonids. Curved black dashed line is GAM smoother of all measured T_{max} for all years 1998-2020, indicating typical conditions for each day of year.

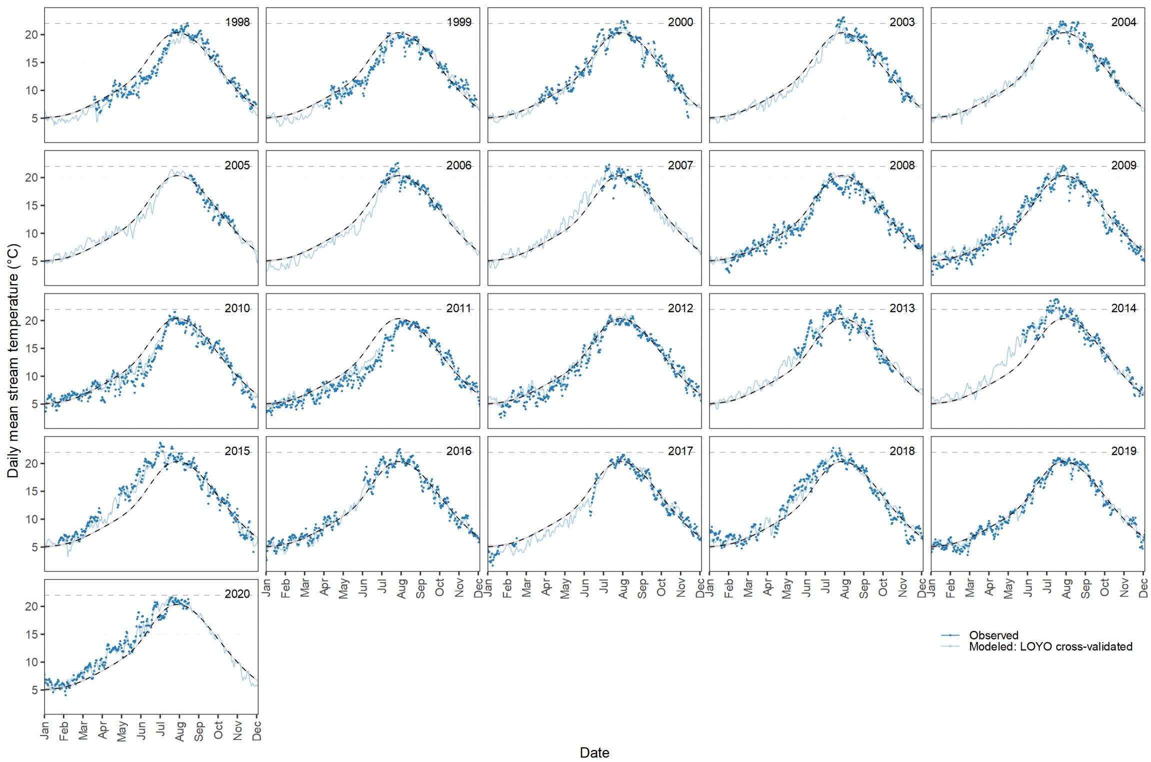

Figure S7. Daily time series of measured (dots) and modeled (solid lines, from leave-one-out [LOYO] cross-validation) T_{mean} in the Scott River at the USGS gage for the years 1998–2020 (no data 2001-2002). Horizontal dashed gray line at 22 °C indicates a temperature threshold for juvenile salmonids. Curved black dashed line is GAM smoother of all measured T_{mean} for all years 1998-2020, indicating typical conditions for each day of year.

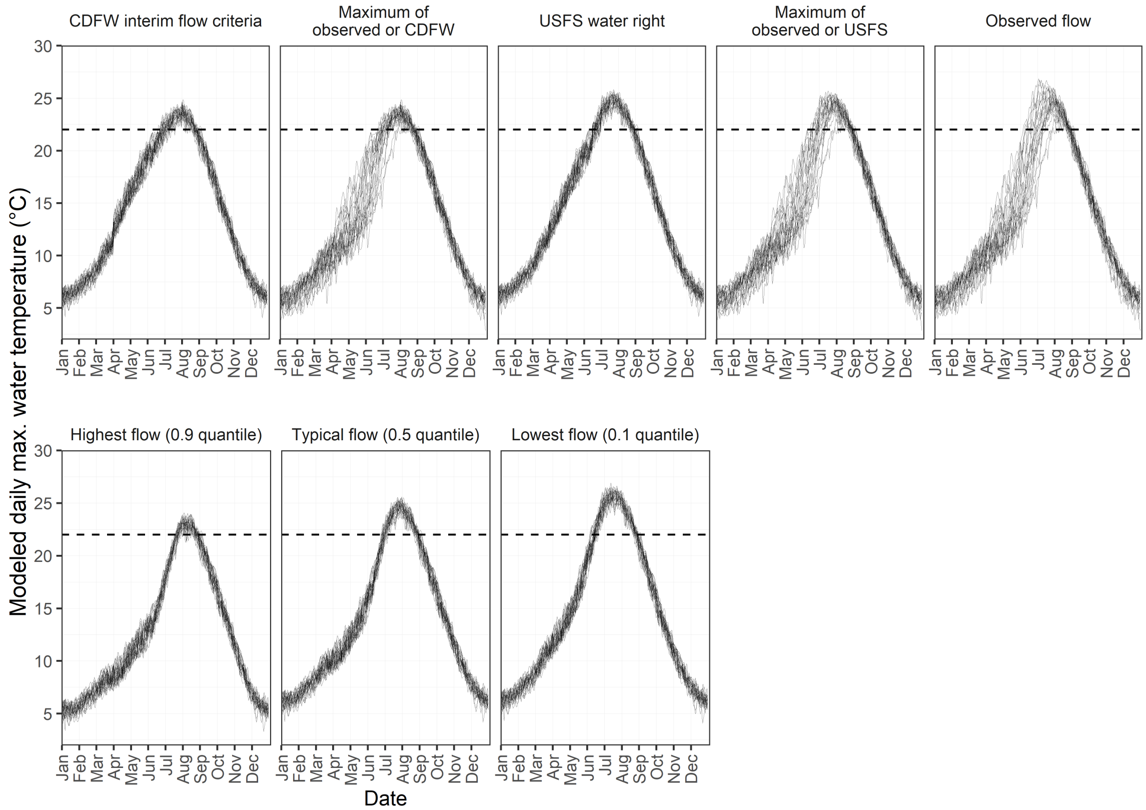

Figure S8. Scott River T_{max} predicted with a statistical model under the group of scenarios that pair observed air temperatures for 1998–2020 with eight different flow conditions (Table 1): observed time series of USGS measured flows, three quantile flow scenarios, and four flow scenarios based on the CDFW interim instream flow criteria and USFS water right. Two scenarios use the exact flows (based on month and day) specified in the CDFW flow criteria and USFS water right, while in the other two the CDFW and USFS flows were replaced by observed USGS flows on dates when the observed flows were higher than the management flows (Table 1). Horizontal dashed gray line at 22 °C indicates a temperature threshold for juvenile salmonids.

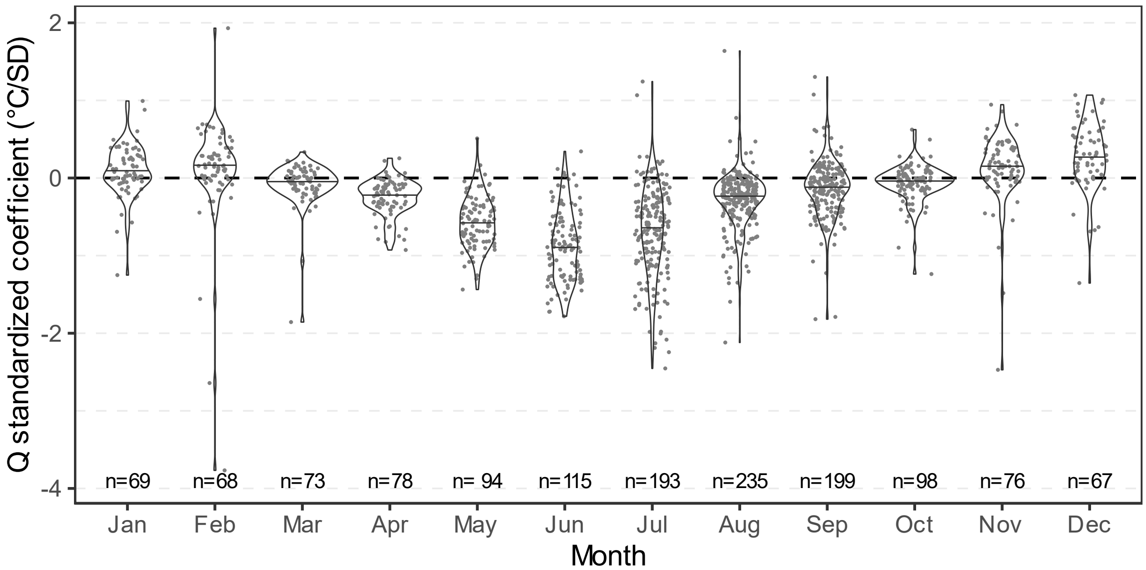

Figure S9. Violin plot (i.e., combination of box plot and density plot) of standardized coefficients for flow (Q) from multiple regression models of monthly stream temperatures at 239 river sites in the Northwestern U.S. where flow is not regulated by dams, from Isaak et al.'s (2018) analysis. Within each month, horizontal lines are median values, gray points are coefficients for individual sites (jittered for legibility), and labels are the number of sites. Isaak et al. (2018) developed these models in the original units of m^3/s. We obtained the coefficients from the study authors, converted the coefficients to standardized units by multiplying each coefficient by the standard deviation of Q for each month and site, and then created this figure.

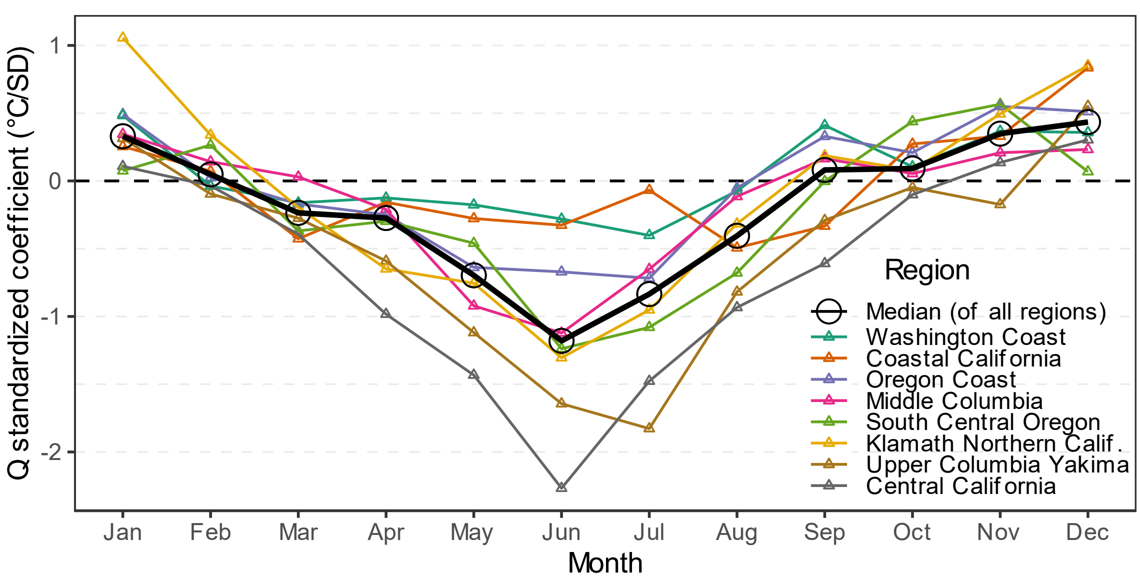

Figure S10. Standardized coefficients for flow (Q) from monthly spatial stream network models of stream temperature in eight Western U.S. regions, from FitzGerald et al.'s (2021) analysis. We created this figure using coefficients provided by the study authors.

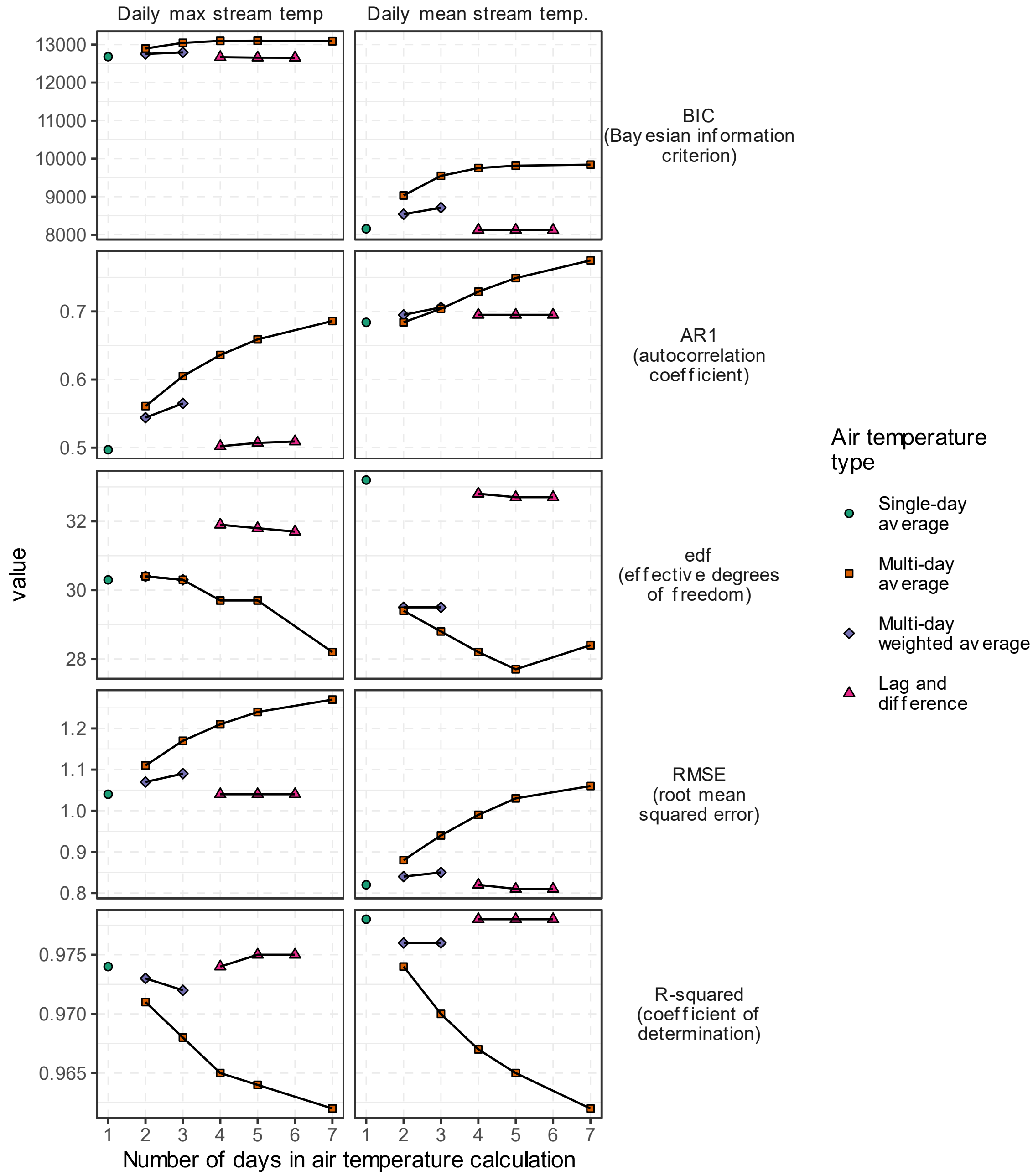

Figure S11. Effect of choice of air temperature metric on model training statistics, comparing 11 models of T_{max} (left panels) and T_{mean} (right panels). Models are alternative versions of the final model “GAM7”, differing only in the choice of the air temperature metric.

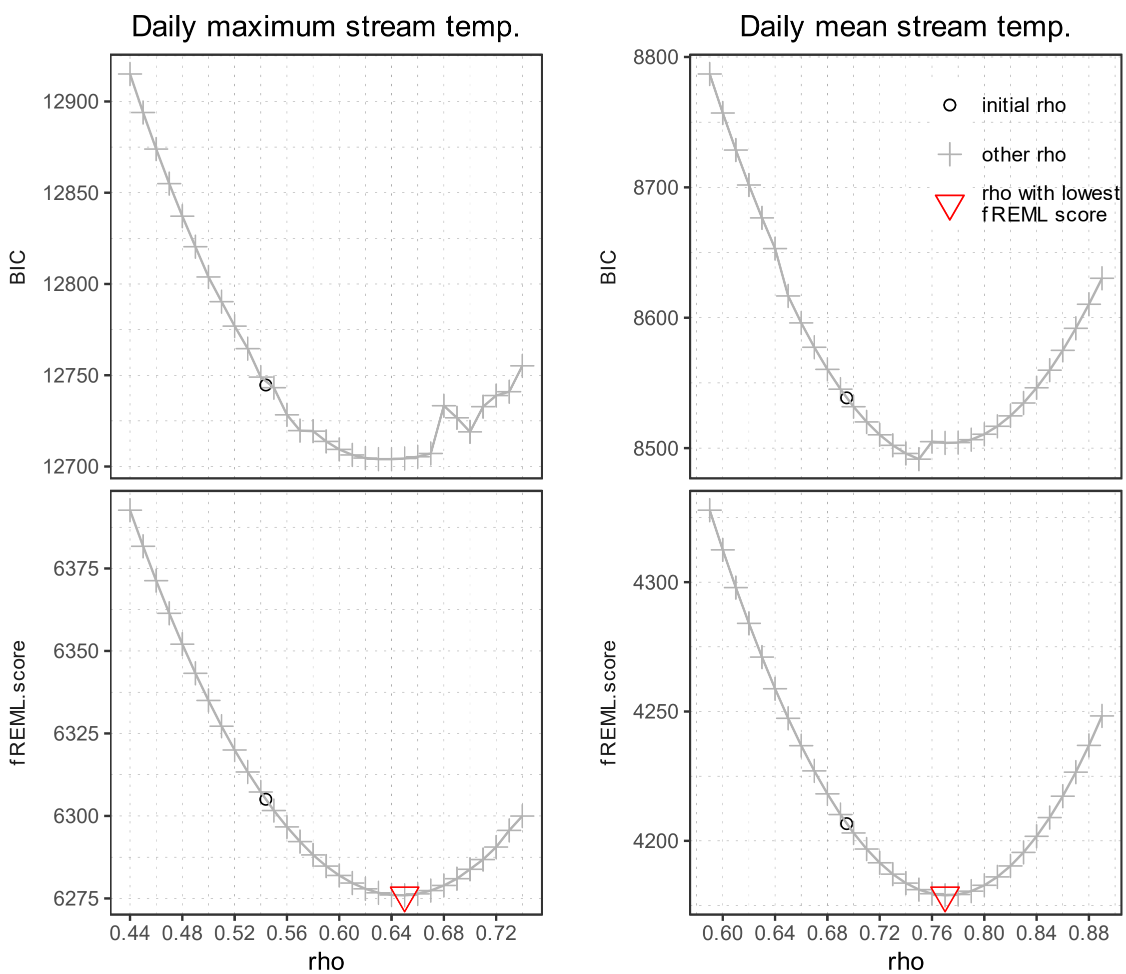

Figure S12. Plots comparing BIC (top panels), and fREML scores (bottom panels) for alternative versions of the Scott River final "GAM7" model for T_{max} (left panels) and T_{mean} (right panels) that use different autocorrelation values (i.e., rho, on x-axis). The "initial" rho value is the lag 1 autocorrelation value of the residuals from an initial model without autocorrelation. "Other" rho values range from 0.1 below the initial value to 0.2 above the initial value, in 0.01 increments.

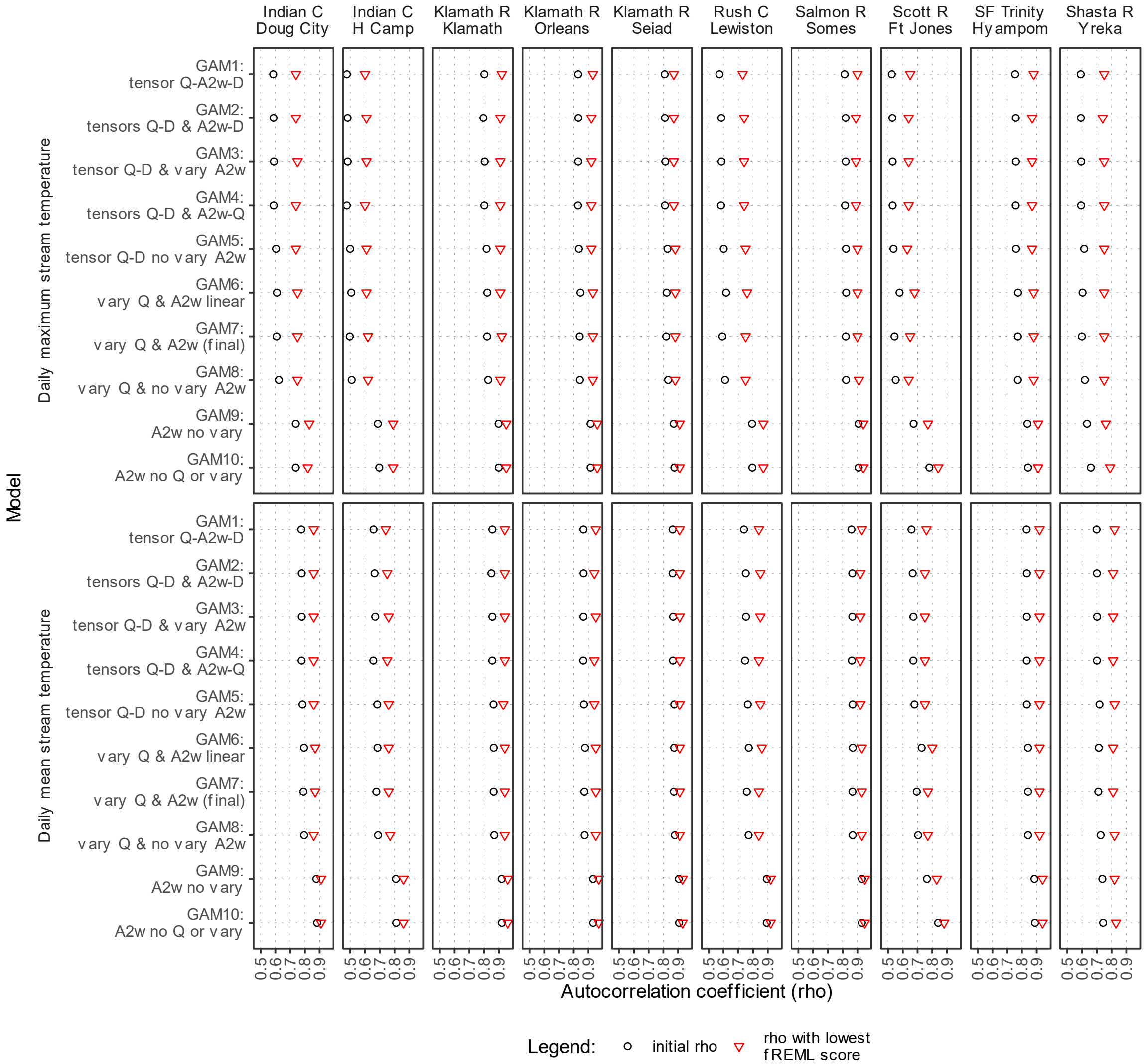

Figure S13. Comparison, for each site and model, of initial rho values and rho values that minimizes the fast restricted maximum likelihood (fREML) score for T_{max} (top panels) and T_{mean} (bottom panels). The "initial" rho value is the lag 1 autocorrelation value of the residuals from an initial model without autocorrelation. GAM11 does not have an autocorrelation coefficient so is not included here.

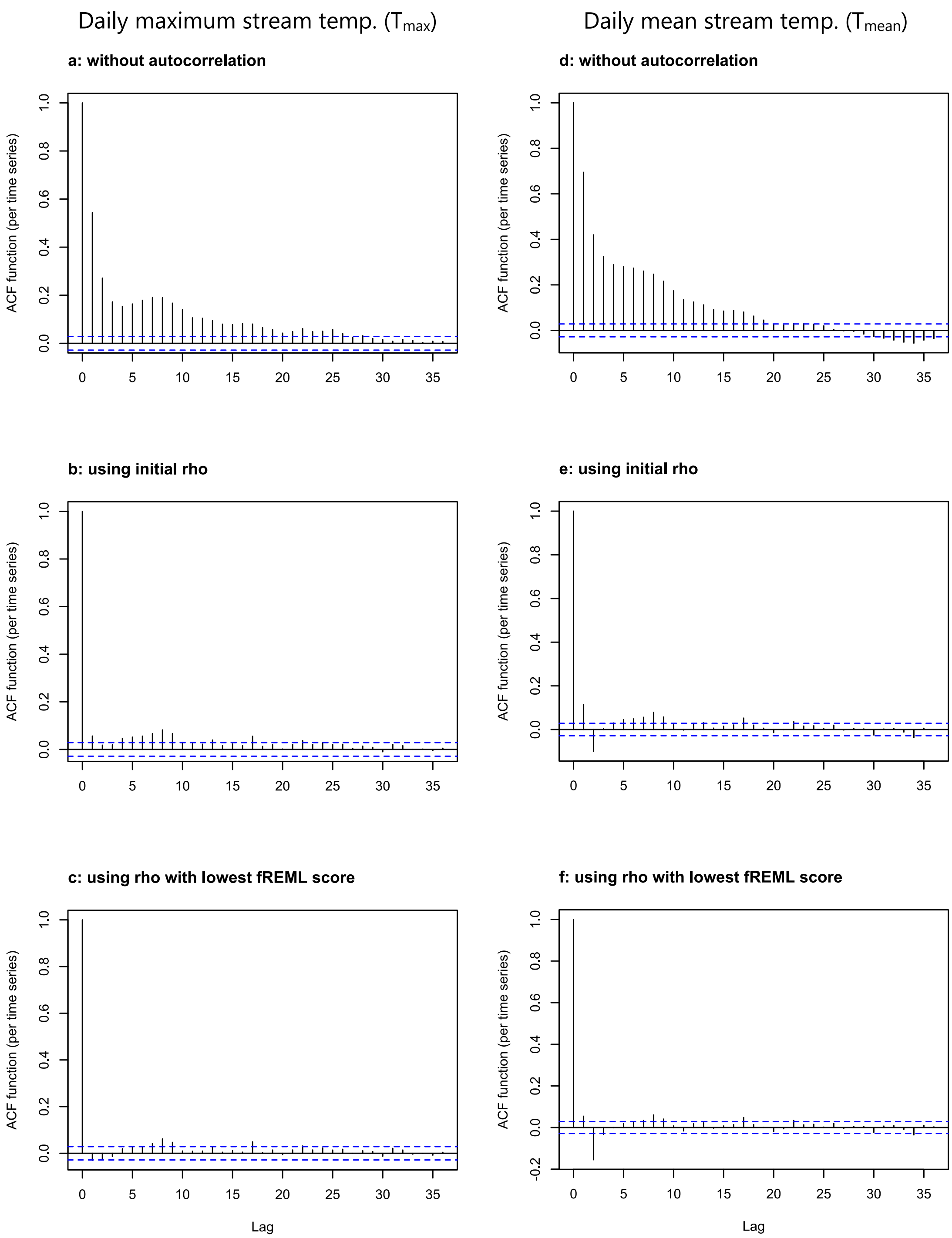

Figure S14. Autocorrelation function (ACF) plots for alternative versions of the Scott River final "GAM7" models for T_{max} and T_{mean} with (a,d) no autocorrelation structure, or autocorrelation values (i.e., rho) set as either (b,e) the lag 1 autocorrelation value of the residuals from an initial model without autocorrelation, or (c,f) the rho value that minimizes the fast restricted maximum likelihood (fREML) score (i.e., red triangle in Figure S12).

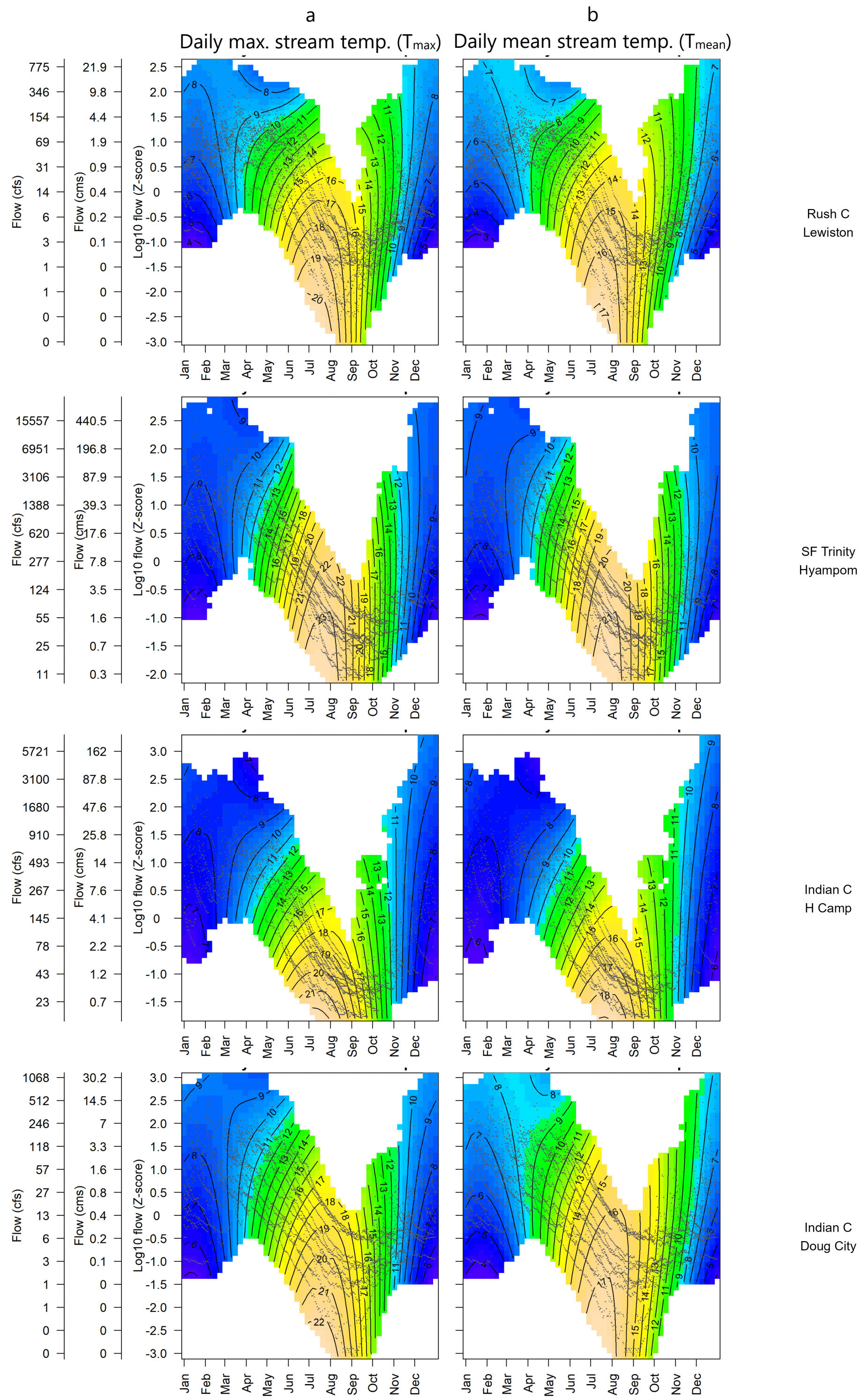

Figure S15. Effects of flow (Q) and day of year (D) on predicted values of (a) T_{max} and (b) T_{mean} in selected model GAM7 at four example sites. Sites in top two rows have non-monotonic relationships in Oct–Nov (Section 5.4) while sites in the bottom two rows do not). Colors and labeled contour lines show predicted temperatures (°C). Underlying gray dots show calibration data. Y-axis labels provide multiple units to facilitate interpretation.